Article

Current Biology

Conflict during learning reconfigures the neural representation of positive valence and approach behavior

Graphical abstract

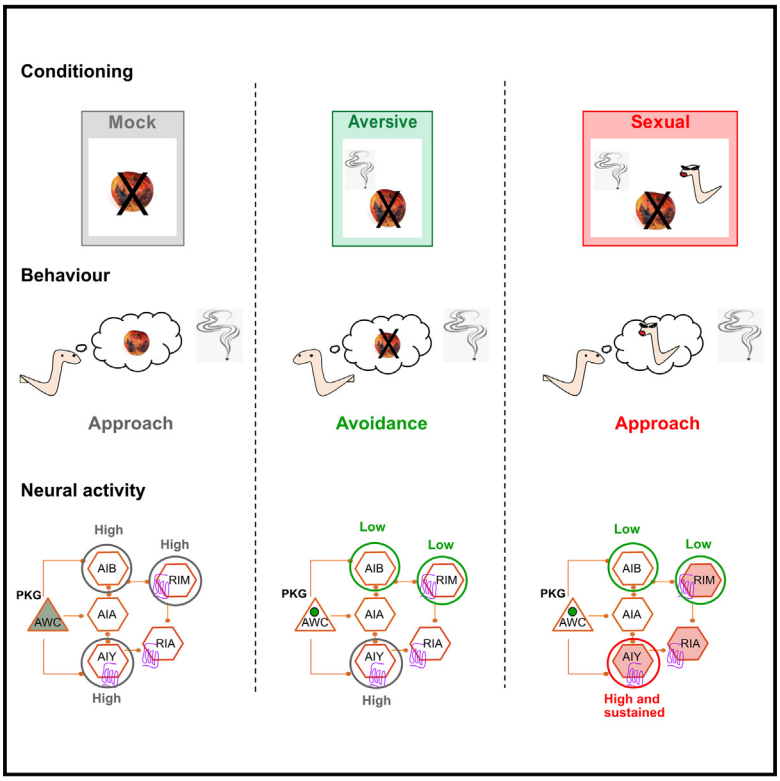

Authors

Laura Molina-García,
Susana Colinas-Fischer,
Sergio Benavides-Laconcha, ...,
Milly Butts, Chris P. Barnes,
Arantza Barrios

Correspondence

laura.molina@cnb.csic.es (L.M.-G.),
a.barrios@ucl.ac.uk (A.B.)

In brief

How are positive and negative experiences integrated during learning? Here, Molina-García, Colinas-Fischer, et al. find that the neuropeptide PDF-1 encodes both experiences by being released from and acting on different cells. Each experience generates a co-existing memory, and this changes the neural representation of positive valence.

Highlights

- Aversive and rewarding experiences are both encoded by PDF-1 neuromodulation
- When presented together, each experience generates a distinct memory
- Positive valence can be encoded by more than one pattern of neural activity
- Stimulus valence is represented according to stimulus prediction

Molina-García et al., 2024, Current Biology *34*, 5470–5483
December 2, 2024 © 2024 The Author(s). Published by Elsevier Inc.
https://doi.org/10.1016/j.cub.2024.10.024

CellPress

CellPress
OPEN ACCESS

Current Biology

Article

Conflict during learning reconfigures the neural representation of positive valence and approach behavior

Laura Molina-García,[1,2,3,4,*] Susana Colinas-Fischer,[1,3] Sergio Benavides-Laconcha,[1] Lucy Lin,[1] Emma Clark,[1] Neythen J. Treloar,[1] Blanca García-Minaur-Ortíz,[1] Milly Butts,[1] Chris P. Barnes,[1] and Arantza Barrios[1,5,*]

[1]Department of Cell and Developmental Biology, University College London, London WC1E 6BT, UK
[2]Present address: Microbial Biotechnology Department, National Centre for Biotechnology (CNB-CSIC), 28049 Madrid, Spain
[3]These authors contributed equally
[4]X (formerly Twitter): @LMolina_Garcia
[5]Lead contact
*Correspondence: laura.molina@cnb.csic.es (L.M.-G.), a.barrios@ucl.ac.uk (A.B.)
https://doi.org/10.1016/j.cub.2024.10.024

SUMMARY

Punishing and rewarding experiences can change the valence of sensory stimuli and guide animal behavior in opposite directions, resulting in avoidance or approach. Often, however, a stimulus is encountered with both positive and negative experiences. How is such conflicting information represented in the brain and resolved into a behavioral decision? We address this question by dissecting a circuit for sexual conditioning in *C. elegans*. In this learning paradigm, an odor is conditioned with both a punishment (starvation) and a reward (mates), resulting in odor approach. We find that negative and positive experiences are both encoded by the neuropeptide pigment dispersing factor 1 (PDF-1) being released from, and acting on, different neurons. Each experience creates a distinct memory in the circuit for odor processing. This results in the sensorimotor representation of the odor being different in naive and sexually conditioned animals, despite both displaying approach. Our results reveal that the positive valence of a stimulus is not represented in the activity of any single neuron class but flexibly represented within the circuit according to the experiences and predictions associated with the stimulus.

INTRODUCTION

Animals need to constantly evaluate the stimuli they encounter to decide to approach, avoid, or ignore them. The valence (i.e., the value and sign) of a stimulus is subjective and depends on genetics, physiological needs, and previous experiences. Some stimuli, such as food odors or mates' pheromones, have positive valence and are innately attractive, whereas other stimuli, such as the smell of a predator, are innately aversive. However, even valence that is innately assigned can be switched through learning and experience.[1,2] For example, the response of male fruit flies to mated females switches from attraction to avoidance after repeated courtship rejection,[3] and *C. elegans* worms learn to avoid the innately attractive bacteria *Pseudomonas aeruginosa* after ingesting this pathogen.[4,5] How is valence appropriately and flexibly assigned? Studies in diverse species have identified specific and segregated circuits dedicated to process positive (approach) and negative (avoidance) valence.[5–8] Such circuits provide information about the motivational state of the animal or about the experiences associated to a stimulus to guide approach or avoidance. However, and with the exception of the gill withdrawal reflex in Aplysia,[9] a fully mapped-out circuit and path of information flow, from the rewarding or punishing experience that modifies the valence assigned to a stimulus to the behavioral decision to approach or avoid it, has not been described. Furthermore, in nature, stimuli are experienced together with positive and negative events. How is this conflict in valence assignment resolved? We address this question by dissecting the circuit mechanisms underlying sexual conditioning in *C. elegans*.

C. elegans worms are innately attracted to many chemical stimuli, including salt and the odor benzaldehyde, which is a bacterial metabolite.[10,11] Innate approach, however, can be switched to learned avoidance after aversive conditioning in which worms experience the stimulus together with a punishment such as starvation.[12–14] An additional switch in preferences has been described in males, for which learned avoidance can be overridden by the presence of mates during conditioning resulting in approach.[15,16] This form of male-specific learning, which is termed sexual conditioning, provides a paradigm to understand how conflicting rewarding and punishing experiences are integrated and resolved to assign valence and guide behavior to a stimulus. Here, we aversively and sexually conditioned the behavior of males to the odor benzaldehyde and asked the following questions: (1) how is information about mate-experience incorporated into the circuit for odor processing? and (2) how does this information change odor processing to guide behavior? Through cell-specific manipulation of

 © 2024 The Author(s). Published by Elsevier Inc.
This is an open access article under the CC BY license (http://creativecommons.org/licenses/by/4.0/).

CellPress
OPEN ACCESS

neuropeptide signaling, imaging of neuronal activity, and behavioral analysis, we identify a circuit modulated by mate experience through the neuropeptide pigment dispersing factor 1 (PDF-1) and show that during sexual conditioning, punishment and reward form two distinct memories. The result of this is that sexually and aversively conditioned animals, although displaying opposite behaviors, have a more similar sensorimotor representation of the odor than sexually conditioned and naive animals, which both display approach. Our findings reveal that the valence of a stimulus is not represented in the activity of any single neuron class but distributed within the circuit and flexibly represented according to experience.

RESULTS

Odor preferences can be sexually conditioned in males

The presence of mates has previously been shown to condition the behavior of males to salt.[15,16] To establish whether male sexual conditioning is a phenomenon generalizable to stimuli of other modalities, we tested conditioning to the odors benzaldehyde and butanone. To optimize our conditioning protocol, we tested several concentrations of benzaldehyde and conditioning times. We determined 15% benzaldehyde for 3 h as the optimal condition that elicits robust aversion to benzaldehyde without producing any toxicity (Table S1). We used controls (starvation without odor or odor with food) that did not change behavior from attraction to repulsion (Figures 1A and 1B). We then tested whether aversive learning could be overridden by the presence of mates during conditioning. Hermaphrodites were repelled by the odor regardless of whether mates (males) had been present or not during conditioning with odor and starvation (Figure 1B). In contrast, males that had been conditioned with odor, starvation, and mates displayed attraction to the odor (Figure 1B). These results show that, as with salt, behavioral responses to odor can be sexually conditioned in males but not in hermaphrodites. Next, we tested male sexual conditioning to butanone. Males were conditioned and assayed at 1:1,000 dilutions of butanone. Similar to what we had observed with benzaldehyde, mock and sexually conditioned males were fully attracted to butanone and aversively conditioned males were strongly repelled (Figure 1C). This supports the idea that for males, who need to mate to reproduce, the presence of mates is a rewarding experience that can modulate the behavioral response to other environmental stimuli[17,18] and even override aversive learning in some instances. We next sought to identify the molecular and cellular mechanisms underlying sexual conditioning.

PDF neuropeptide signaling regulates aversive learning and sexual conditioning

Sexual conditioning to salt is regulated by the neuropeptide PDF-1.[16] We therefore tested whether mutants for *pdf-1*, for the PDF-1 receptor *pdfr-1*, and for a second ligand, *pdf-2*,[19,20] had altered behavioral responses to odor. To determine whether a genotype was proficient or defective at learning, we compared the frequency distribution of chemotaxis scores between conditions. We made two comparisons: one across genotypes comparing mutant and wild-type worms for a given conditioning treatment and another within genotype comparing mock with aversive conditioning and aversive with sexual conditioning (see STAR Methods). As previously reported for sexual conditioning to salt,[16] *pdf-1(tm1996)* mutants exhibited a defect in sexual conditioning to odor compared with wild-type males. Although chemotaxis scores were shifted toward more positive values compared with aversively conditioned worms, the scores were distributed across all possible categories and mainly concentrated around 0, indicating a lack of preference for the odor (Figure 1D). *pdf-1* mutants were defective for sexual conditioning specifically and displayed naive and aversive responses equivalent to those of wild-type animals (Figure 1D). Surprisingly, *pdfr-1(tm4457)* receptor mutants were defective in both sexual conditioning and aversive learning. Although the chemotaxis scores of *pdfr-1* mutants shifted toward lower values after aversive conditioning, most animals displayed a lack of preference—or even some residual attraction—and this similar distribution was maintained after sexual conditioning (Figure 1D). To establish whether aversive learning is mediated by another PDF ligand, we tested the responses of *pdf-2* single and *pdf-1; pdf-2* double mutants. *pdf-2 (tm4393)* mutants did not differ from wild-type animals in either aversive learning or sexual conditioning (Figure 1D). In contrast, *pdf-1(tm1996); pdf-2(tm4393)* double mutants lacking both PDF ligands displayed similar defects to *pdfr-1* receptor mutants in both aversive learning and sexual conditioning (Figure 1D). Altogether, these data show that both PDF-1 and PDF-2 are sufficient for full aversive learning but only PDF-1 is required to modulate odor preferences toward full attraction after sexual conditioning.

PDF signaling acts on different neurons to drive odor avoidance or approach after learning

Next, we asked which cells respond to PDF-1 neuromodulation to effect sexual conditioning. We generated rescue constructs that express wild-type *pdfr-1* cDNA in *pdfr-1* mutant animals using two *pdfr-1* promoters that drive expression in different groups of neurons[21,22] (Figures 2A and 2B). The proximal promoter drove expression in neurons and body muscle[21] (Figure 2B). The distal promoter drove Cre-dependent conditional expression of the receptor[22] (Figure 2B).

Expression of *pdfr-1* under the proximal promoter fully rescued odor avoidance in *pdfr-1* mutants after aversive learning (Figure 2C). After sexual conditioning, transgene-carrying mutants displayed a frequency distribution of chemotaxis scores that was not significantly different from that of *pdfr-1* mutants. However, their scores were shifted toward more positive values compared with those displayed after aversive learning, indicating a loss of aversion and, therefore, a partial rescue of sexual conditioning (Figure 2C). Restoring expression of *pdfr-1* from the distal promoter with a panneuronal Cre line fully rescued odor attraction in *pdfr-1* mutants after sexual conditioning, with a distribution of chemotaxis scores not significantly different from that of wild-type worms (Figure 2D). This construct, however, did not rescue odor avoidance after aversive conditioning and worms displayed lack of preference, similar to *pdfr-1* mutants (Figure 2D). Together, these data suggest that the PDFR-1 receptor is required in different neurons to drive either aversion or attraction to the odor after learning.

The distal, but not the proximal, *pdfr-1* promoter has been shown to drive expression in the interneurons ring interneuron

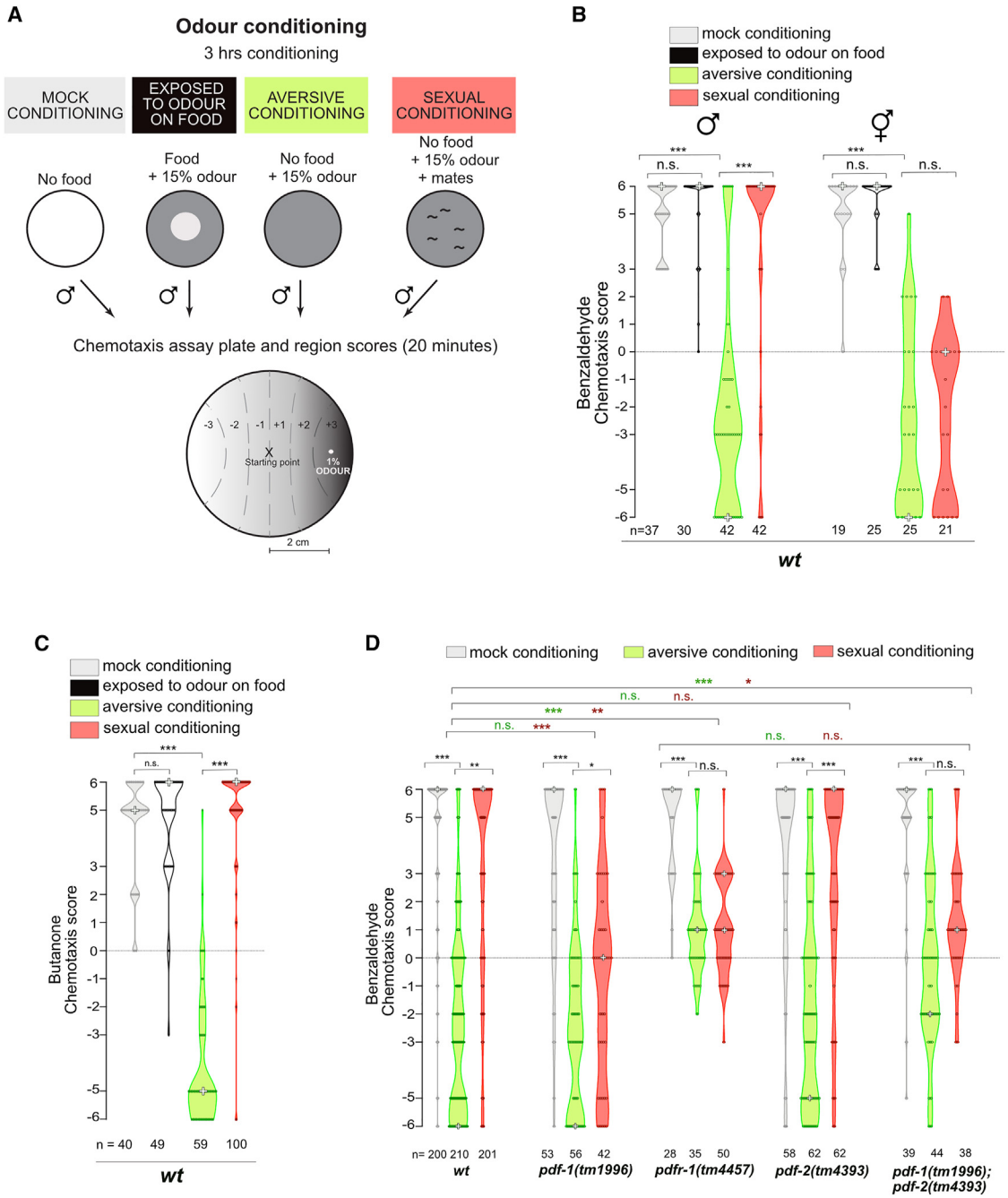

Figure 1. PDF neuropeptide signaling regulates aversive learning and sexual conditioning to odor

(A) Odor conditioning paradigm.

(B–D) (B and D) Chemotaxis scores to benzaldehyde and (C), to butanone, after conditioning. χ^2 for trend test was used to compare between conditions and genotypes. White cross represent the mode. Black asterisks correspond to comparisons between conditions within genotype; green and red asterisks correspond to comparisons between genotypes for aversive and sexual conditioning, respectively. ***$p < 0.001$; **$p < 0.01$; *$p < 0.05$; n.s., no statistically significant difference $p \geq 0.05$. *n*, number of animals. See also statistical analysis section of STAR Methods.

See also Table S1.

M (RIM), ring interneuron A (RIA), and anterior interneuron Y (AIY).[22] These neurons are part of the circuit for odor processing[23,24] and have been implicated in naive and learned behavioral responses to other sensory stimuli.[5,25,26] We used the *tdc-1*,[22] *glr-3*,[22,27] and *ttx-3*[28] promoters to drive expression of Cre recombinase in RIM, RIA, and AIY, respectively. Expression of *pdfr-1* in RIM, RIA, and AIY together partially rescued odor attraction after sexual conditioning (Figure 2D). After aversive learning, the scores of transgene-carrying *pdfr-1* mutants remained distributed across all possible categories and mainly

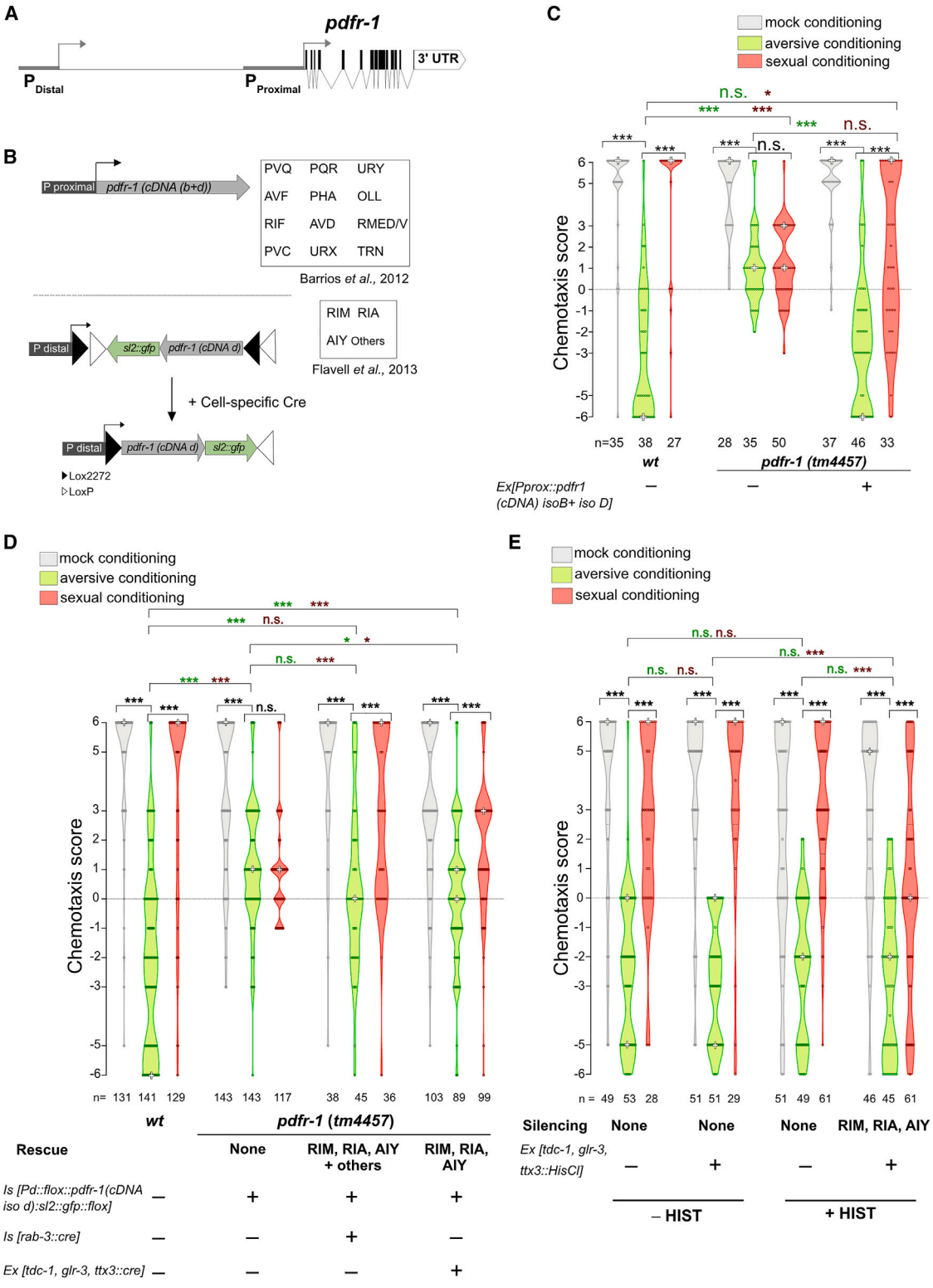

Figure 2. PDFR-1 is required in different neurons for learned approach and learned avoidance

(A) Genomic locus of the *pdfr-1* gene.

(B) DNA constructs to rescue expression of the *pdfr-1* gene.

(legend continued on next page)

concentrated around 0, indicating a lack of preference for the odor (Figure 2D). These results indicate that odor attraction after sexual conditioning, but not odor avoidance after aversive learning, requires modulation of RIM, RIA, and AIY by PDF-1. We further confirmed the requirement of RIM, RIA, and AIY in learned odor attraction by silencing them with a histamine-gated chloride channel transgene HisCl1[29] during conditioning. Silencing resulted in males that displayed no preference for the odor after sexual conditioning and had intact naive and aversive responses (Figure 2E).

PDF-1 is required in the interneurons AVB and MCM to mediate sexual conditioning

We next asked which neurons are important sources of PDF-1 to mediate odor attraction after sexual conditioning. Two *pdf-1*-expressing neurons that receive inputs from mate-sensing circuits were identified as good candidates to incorporate information about mate experience into the odor circuit: the sex-shared anterior ventral process B (AVB) interneurons and the male-specific mystery cells of the male (MCM) interneurons (previously implicated in sexual conditioning to salt)[16,17,30–33] (Figures 3A and 3B). To remove *pdf-1* with cell selectivity, we generated a single copy insertion of a Lox P-flanked *pdf-1* transgene[22] (Figure 3C), which fully rescued the sexual conditioning defects of *pdf-1(tm1996)* mutants (Figure 3D). Cre-dependent excision of *pdf-1* from MCM interneurons resulted in a significant shift in the distribution of chemotaxis scores of sexually conditioned animals toward more negative values and across all categories (Figure 3D). Removing *pdf-1* from AVB interneurons resulted in males that failed to undergo sexual conditioning and displayed a similar distribution of chemotaxis scores after sexual conditioning and after aversive learning (Figure 3D). In contrast, removing *pdf-1* from the sublateral interneuron A ventral (SIAV) interneurons, which, unlike MCM and AVB neurons, do not receive any synaptic input from mate-sensing circuits,[30] did not result in any defects in naive or learned odor preferences (Figure 3D). These results demonstrate that sexual conditioning requires PDF-1 from both male-specific MCM and sex-shared AVB interneurons.

Next, we tested whether MCM and AVB neurons are also required sources of PDF-1 during aversive learning, which is mediated by both PDF-1 and PDF-2. For this, we carried out cell-specific removal of *pdf-1* in a *pdf-1(tm1996); pdf-2(tm4393)* double-mutant background. We found that removing *pdf-1* from either MCMs or AVBs had no effect on the odor avoidance responses of aversively conditioned animals (Figure S1). Together, these data show that PDF-1 conveys different information within the circuit for odor processing, depending on its source of release.

AVB interneurons are activated by mate sensation

If the MCM and AVB interneurons incorporate information about mate experience into the circuit for odor processing through the release of PDF-1, we would expect them to become activated by mate sensation during conditioning. To test this, we measured changes in intracellular Ca^{2+} (as a proxy for neuronal activation) during conditioning. We used the *pdf-1* promoter to drive expression of the calcium indicator calcium-modulated photoactivatable ratiometric integrator (CaMPARI), which irreversibly photoconverts from green to red upon blue light stimulation at high levels of intracellular Ca^{2+}.[34] We induced photoconversion during conditioning and then measured and compared levels of photoconversion in AVB and MCM neurons of animals that had been conditioned with odor and lack of food in the absence or presence of mates (Figure 3E). Consistent with the hypothesis that mate sensation activates the AVB neurons, we saw high levels of photoconversion in AVB neurons only if mates were present during conditioning (Figure 3E). In contrast, and opposite to our expectations, we did not observe an increase in Ca^{2+} levels in MCM neurons (Figure 3E).

AVB activity is highly correlated with forward movement.[35,36] We confirmed that AVB activation during conditioning was specifically due to mate sensation, rather than to an increase in forward movement, with two additional experiments. We compared the proportion of time that males spent moving forward and backward during mock, aversive, and sexual conditioning. As expected for males engaged in the mating sequence, males in sexual conditioning plates spent a significantly higher proportion of their time moving backward compared with males in mock and aversive conditioning plates (Figure S2A). Second, we measured CaMPARI photoconversion in the AVB neurons of tail-defective *mab-3* mutant males during conditioning. *mab-3* males fail to develop rays 1–6 (sensory structures required for sensing mates) and are unable to undergo sexual conditioning[15] (Figure S2B). We observed similarly low levels of photoconversion in *mab-3* mutant males regardless of whether mates were present or not during conditioning (Figure 3E). This result supports the idea that AVB activation requires mate contact and drives sexual conditioning.

The lack of CaMPARI photoconversion in the MCM neurons led us to seek further evidence of their involvement in sexual conditioning. We used a temperature-sensitive mutant isolated in the Poole lab, *nom-8 (drp-8)*, which fails to develop MCM neurons at 25°C. When raised at the permissive temperature (20°C), *nom-8* mutants were proficient at naive and learned behavioral responses to odor (Figure S2C). In contrast, when raised at the restrictive temperature (25°C), which results in lack of MCM interneurons, *nom-8* mutants failed to undergo sexual conditioning and displayed a distribution of chemotaxis scores that were negative and no different from those displayed after aversive learning (Figure S2C). Although raising animals at 25°C resulted in a slight shift of chemotaxis scores toward lower values in mock and sexually conditioned animals of both genotypes (Figure S2C), sexual conditioning was severely impaired only in *nom-8* mutants. Altogether, these experiments demonstrate that AVB interneurons are activated by mate sensation during sexual conditioning. PDF-1 neuropeptide released from AVB neurons modulates the circuit for odor processing to switch subsequent behavior from odor avoidance to approach.

(C–E) Chemotaxis scores to benzaldehyde after conditioning. *pdfr-1(tm4457)* data in (C) are the same as in Figure 1C. White cross represents the mode. χ^2 for trend test was used to compare between conditions and genotypes. Black asterisks correspond to comparisons between conditions within genotype; green and red asterisks correspond to comparisons between genotypes for aversive and sexual conditioning, respectively. ***$p < 0.001$; **$p < 0.01$, *$p < 0.05$, n.s., no statistically significant difference $p \geq 0.05$. *n*, number of animals. See also statistical analysis section of STAR Methods.

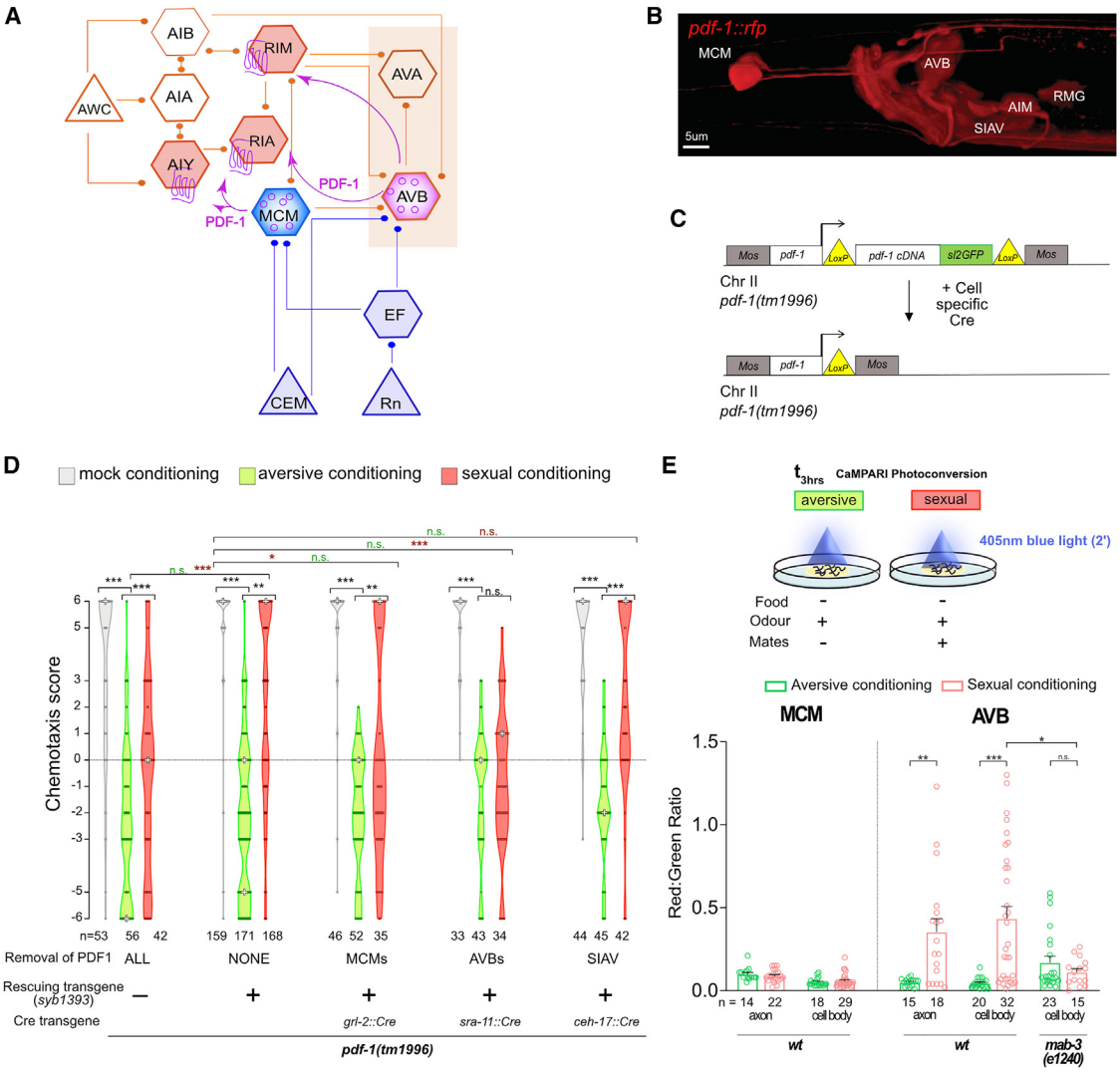

Figure 3. The MCM and AVB interneurons are a source of PDF-1 for sexual conditioning

(A) Circuit for odor processing in males. Triangles, hexagons, and circles represent sensory neurons, interneurons, and PDF-1, respectively. Synaptic connections are depicted as lines and peptidergic communication as arrows. Male-specific neurons are shown in blue. Neuron names are indicated.

(B) Lateral view (anterior to the left) of the anterior-most part of a male expressing a *pdf-1::rfp* reporter.

(C) Scheme of the excisable single copy *pdf-1* transgene integrated by Mos-1 mediated single-copy insertion (MosSCI) in chromosome II.

(D) Chemotaxis score to benzaldehyde after conditioning. Data for *pdf-1(tm1996)* mutants are the same as in Figure 1C. White cross represents the mode. χ^2 for trend test was used to compare between conditions and genotypes. Black asterisks correspond to comparisons between conditions within genotype; green and red asterisks correspond to comparisons between genotypes for aversive and sexual conditioning, respectively. ***$p < 0.001$; **$p < 0.01$; *$p < 0.05$; n.s., no statistically significant difference $p \geq 0.05$. See also statistical analysis section of STAR Methods.

(E) CaMPARI photoconversion experiment. A non-parametric two tail Mann Whitney-U test was performed. Each circle represents a neuron. ***$p < 0.001$; **$p < 0.01$; *$p < 0.05$; n.s., no statistically significant difference $p \geq 0.05$. Error bars represent SEM. *n*, number of neurons.

Also see Figures S1 and S2.

Furthermore, our results suggest that although the MCM interneurons are required for the modulation of odor preferences by mate sensation, their activation may not be reflected as changes in intracellular Ca^{2+} levels.

The aversive memory forms in both aversively and sexually conditioned animals

Our data show that starvation and mate sensation act as punishing and rewarding experiences, respectively, which condition odor preferences in opposite directions: avoidance versus approach (Figures 4A and S3A). However, sexual conditioning in which the odor is presented with both starvation and mates results in clear odor approach. How does the presence of mates override the behavioral consequences of aversive learning? We postulated two alternative models (Figure 4B). In model 1, the presence of mates inhibits the formation of the aversive memory in which odor predicts starvation. In this model, only the rewarding memory in which odor predicts mates is formed.

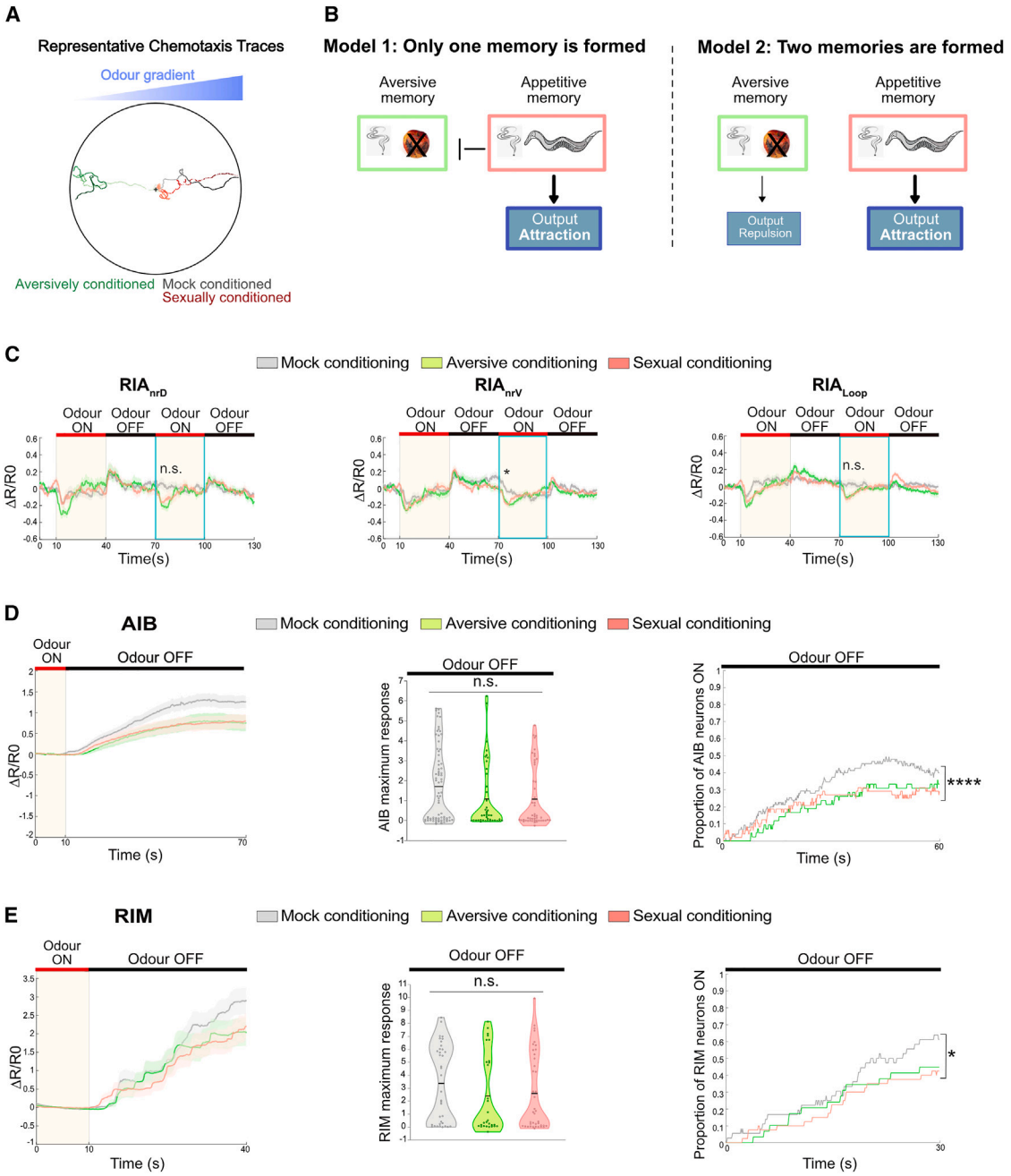

Figure 4. The aversive memory is also formed during sexual conditioning

(A) Tracks of conditioned worms chemotaxing. Black cross indicates approximate starting point.

(B) Proposed models for integration of punishment and reward during sexual conditioning.

(C) Odor-evoked GCaMP6f/red fluorescent protein (RFP) fluorescence ratios in RIA interneurons after conditioning.

(D and E) (D) AIB and (E), axonal RIM activity. Left, odor-evoked GCaMP6f/RFP fluorescence ratios. A non-parametric one-way ANOVA with Dunn's multiple comparisons was used to compare between conditions; middle, maximum activity during odor removal (each circle represents one neuron). A non-parametric ANOVA was used to compare between conditions; right, proportion of neurons active at each time point during odor removal. A binary logistic regression and ANOVA was used to compare between conditions. ****$p < 0.0001$; *$p < 0.05$; n.s., no statistically significant difference $p \geq 0.05$. Shaded areas in odor-evoked GCaMP6f/RFP fluorescence ratios graphs represent SEM. Solid lines represent the mean of activity of the neuronal population tested (see also statistical analysis section of STAR Methods).

Also see Figure S3.

Alternatively, in model 2, the presence of mates creates an additional reward memory that co-exists with the aversive memory. Because memories can be identified as biophysical changes in the brain, to distinguish between the two models, we monitored and compared odor-evoked neuronal responses after conditioning. The prediction was that in aversively conditioned animals we would observe evidence of an aversive memory having formed as changes in neural activity within the circuit compared with naive animals. Such changes would be absent in sexually conditioned animals if model 1 was correct but present if model 2 was correct instead.

We measured odor-evoked neuronal activity with the Ca^{2+} indicator GCaMP6f in an olfactory chip.[37,38] We monitored 4 classes of interneurons (AIY, anterior interneuron B [AIB], RIM, and RIA), which act postsynaptically to the odor-sensing neuron amphid wing neuron C (AWC) (Figure 3A) and control navigation in an odor gradient by driving forward movement (AIY) or reorientations (AIB, RIM, and RIA).[23,24,39–41] Moreover, three of them (AIY, RIM, and RIA) receive PDF-1 neuromodulation during sexual conditioning and are required for learned attraction (Figures 2D and 2E). RIA interneurons have three axonal domains (dorsal [nr_d], ventral [nr_v], and sensory loop) that display coordinated odor-evoked activity.[40] We observed a fall and rise in Ca^{2+} upon odor presentation and removal, respectively, in naive and conditioned animals (Figure 4C). However, upon a second round of stimulation, RIA responses in the ventral loop became rapidly adapted in naive animals but not in aversively or sexually conditioned animals (Figure 4C). Although this change is subtle and its impact on behavior unclear, it reveals a memory trace that is linked to both aversive and sexual conditioning.

At rest, AIB and RIM alternate between high and low activity states[24] (Figures S3B and S3C). Although odor presentation inhibits and odor removal activates AIB and RIM, these responses are constrained by the activity state (high or low) that the neuron is in when stimulated.[23,24] To examine AIB and RIM odor-evoked responses, we classified the neurons according to their activity state at the time of odor removal (see STAR Methods). In naive males, AIB was activated by odor removal (Figure 4D). In conditioned animals, in contrast, odor-evoked AIB responses were reduced. We observed a trend toward lower amplitude responses and a significant reduction in the number of neurons that responded to odor removal. This was observed in both aversively and sexually conditioned animals, consistent with model 2 in which the aversive memory is also formed during sexual conditioning (Figure 4D). Similar observations were obtained for the axon of RIM interneurons. The number of RIM neurons that responded to odor removal was significantly reduced in both aversively and sexually conditioned animals compared with naive (Figure 4E). The reduction in the proportion of AIB and RIM neurons becoming active was specific to odor-evoked responses because there was no difference in the proportion of neurons that were in a high activity state at rest, prior to odor exposure, in conditioned and naive animals (Figures S3D and S3E). Together, these results show that the memory formed during aversive learning, by pairing odor with starvation and characterized by a reduction in odor-evoked responses in AIB and RIM, is also formed during sexual conditioning.

Two additional experiments ruled out an alternative interpretation: that the observed changes in AIB and RIM activity reflect a change in motor state independent of odor sensation. Indeed, previous experiences can impact behavioral states and modulate locomotion during exploration independent of stimulus presentation and memory retrieval.[42] First, we confirmed that AIB and RIM are required for the formation of a fully aversive memory. Silencing AIB and RIM with a HisCl1 transgene during conditioning resulted in a significant shift in chemotaxis scores toward more positive values, mainly concentrated around 0 in aversively conditioned animals (Figure 5A). Second, we confirmed that aversive learning does not significantly alter the animal's locomotion state. We measured and compared the length and frequency of reversals, locomotion parameters regulated by AIB and RIM, in conditioned worms exploring in the absence of odor. We found no significant differences between mock and aversively conditioned animals (Figures 5B and S3F) despite significantly different odor-evoked responses in AIB and RIM between these conditions (Figures 4D and 4E). In sexually conditioned animals, we did observe a significant increase in the frequency of reversals during exploration (Figures 5B and S3F), which is consistent with the impact that mate experience has on male behavioral state: increased dwelling.[21,43]

To strengthen our observations that aversive memories are also formed in sexually conditioned animals, we assessed nuclear translocation of the cyclic guanosine monophosphate (cGMP)-dependent protein kinase PKG/EGL-4 in the odor-sensing neuron AWC, a cellular signature of aversive odor learning.[44,45] We measured the sub-cellular localization of PKG/EGL-4 with a transgene driving expression of a GFP-tagged EGL-4 in AWC.[44] Consistent with the idea that the aversive memory is formed also during sexual conditioning, we observed a similar proportion of AWC neurons with EGL-4 nuclear localization in aversively (84.1%) and sexually (76.5%) conditioned animals (Figure 5C; Table S3). In contrast, only 25% and 13% of AWC neurons displayed EGL-4 nuclear localization in naive and control animals exposed to odor while on food, respectively (Figure 5C; Table S3).

Altogether, these data argue against model 1, which proposes that the presence of mates during conditioning inhibits the formation of the aversive memory, and in favor of model 2.

Reward and punishment form two co-existing memories during sexual conditioning

Next, we asked whether a reward memory associated with mate experience also forms during sexual conditioning. We imaged neural activity in AIY neurons, which promote forward movement.[41,46,47] The ventral domain (zone 2) of the axon of AIY interneurons responds to odor stimulation with a rise in Ca^{2+} levels.[23] We did not observe any significant difference between naive and aversively conditioned groups, both of which displayed a rise in Ca^{2+} in AIY axons upon odor presentation (Figures 6A and 6B). In sexually conditioned animals, however, we observed a qualitative change in the responses of AIY. In a significant proportion of animals (39%), the initial Ca^{2+} increase that was normally observed in the other conditions was followed by a second, delayed peak of higher magnitude (maximum peak at least 15 s after odor exposure and R-Rmin/Rmax > 0.4) during odor ON (Figures 6A and 6B). This type of sustained response, which we termed type 2 response (Figure S4A), was significantly less represented in naive (21%) and aversively conditioned (17%)

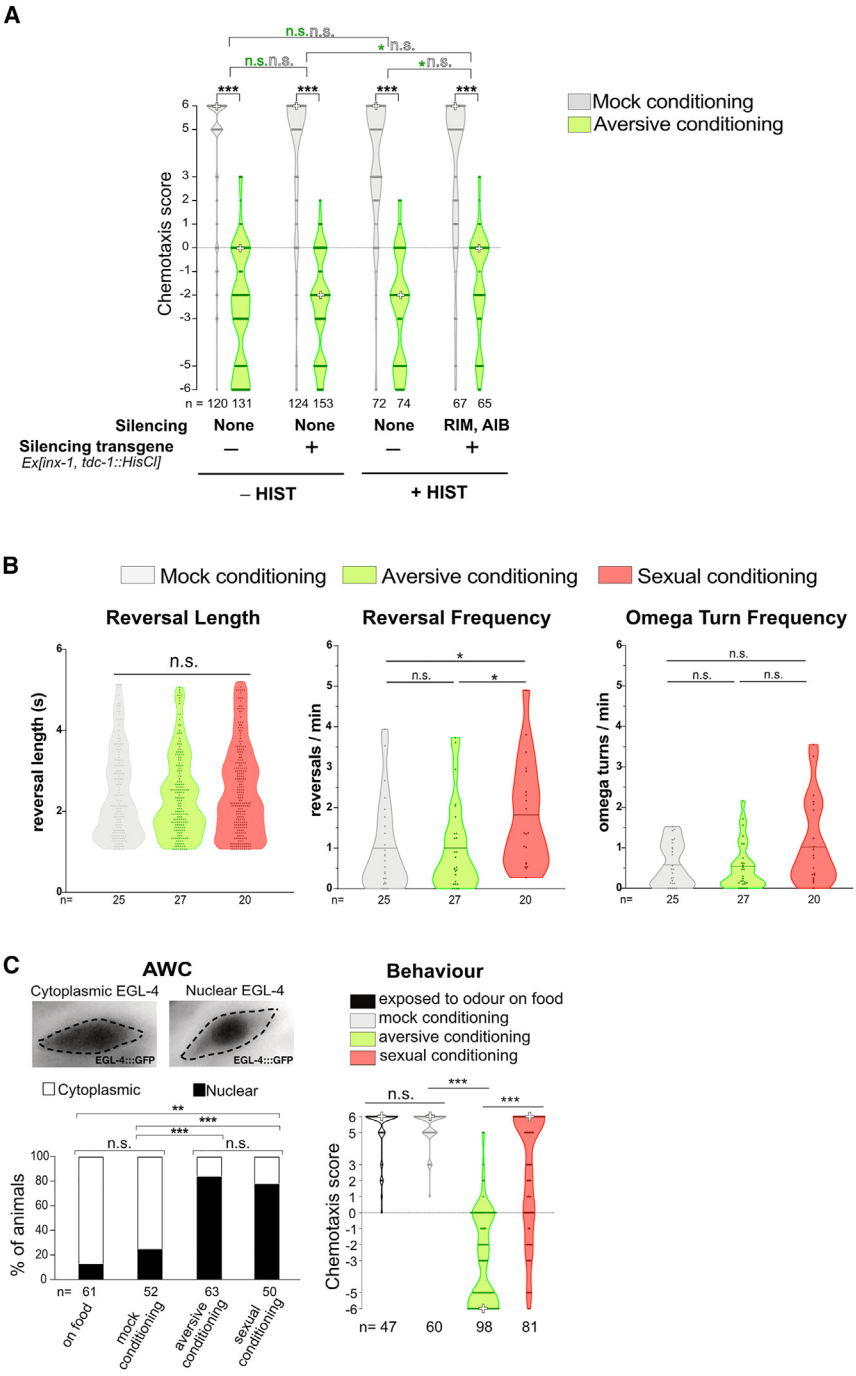

Figure 5. Impact of aversive learning on the circuit for odor sensing

(A) Chemotaxis score to benzaldehyde after conditioning for wild-type males and males with silenced RIM and AIB interneurons. White cross represents the mode. χ^2 for trend test was performed to compare between conditions and genotypes. Black asterisks correspond to comparisons between conditions within genotype; green and grey asterisks correspond to compariosns between genotypes for aversive and mock conditioning, respectively. ***$p < 0.001$; n.s., no statistically significant difference $p \geq 0.05$. *n*, number of animals.

(B) Locomotion parameters of conditioned worms exploring in the absence of odor. For comparing reversal and omega turn frequency, a non-parametric ANOVA (Kruskal-Wallis) test with multiple comparisons was performed. For comparison of reversal length, a χ^2 for trend analysis was used using the deciles of mock reversals as bin edges to determine categories. Each circle represents an event and black lines represent the mean. *$p < 0.05$; n.s., no statistically significant difference $p \geq 0.05$. *n*, number of animals.

(C) EGL-4::GFP localization in AWC neurons after conditioning and chemotaxis score of animals carrying the *odr-3::egl-4::gfp* transgene. White cross represents the mode. χ^2 for trend test was performed to compare the chemotaxis score between conditions and genotypes. Black asterisks correspond to comparisons between conditions within genotype. A χ^2 test was used to compare EGL-4 nuclear translocation between conditioning groups, ***$p < 0.001$; n.s., no statistically significant difference $p \geq 0.05$. *n*, number of animals.

See also Table S3.

animals (Figures 6B and 6C), suggesting that it may be a signature of sexual reward. As sexual reward is conveyed by the neuropeptide PDF-1, and AIY responds to PDF-1 to drive odor approach after sexual conditioning (Figures 1D and 2D), we hypothesized that if AIY type 2 responses were a signature of the rewarding memory, they would be dependent on PDF-1. Indeed, in sexually conditioned *pdf-1 (tm1996)* mutant males, the proportion of AIY type 2 responses was significantly reduced to levels similar to those of mock and aversively conditioned animals (Figures 6A–6C and S4).

Sustained activity in AIY can lead to robust attraction despite reduced activity in AIB

Our data show that during sexual conditioning, an aversive memory and a rewarding memory are formed and compete for behavioral expression. How do these memories drive approach instead of avoidance? We made some predictions based on what is known about the motor output of the neurons in the odor circuit.[23,24,41,45] A reduction of AIB and RIM activity may result in a reduction in the probability of reorientation when the animal is moving down the odor gradient. Although such lack of reorientations cannot account for the avoidance displayed by aversively conditioned animals, it may result in lack of preference. The inability to reorient may be compensated in sexually conditioned animals by sustained and high activity of AIY, which may result in longer forward movement when the animal is moving up the gradient. To test this hypothesis, we built a simplified ordinary differential equation model of the odortaxis circuit, including only the sensory neuron (AWC) and the first layer of postsynaptic interneurons (AIB, AIA, and AIY). We used

CellPress
OPEN ACCESS

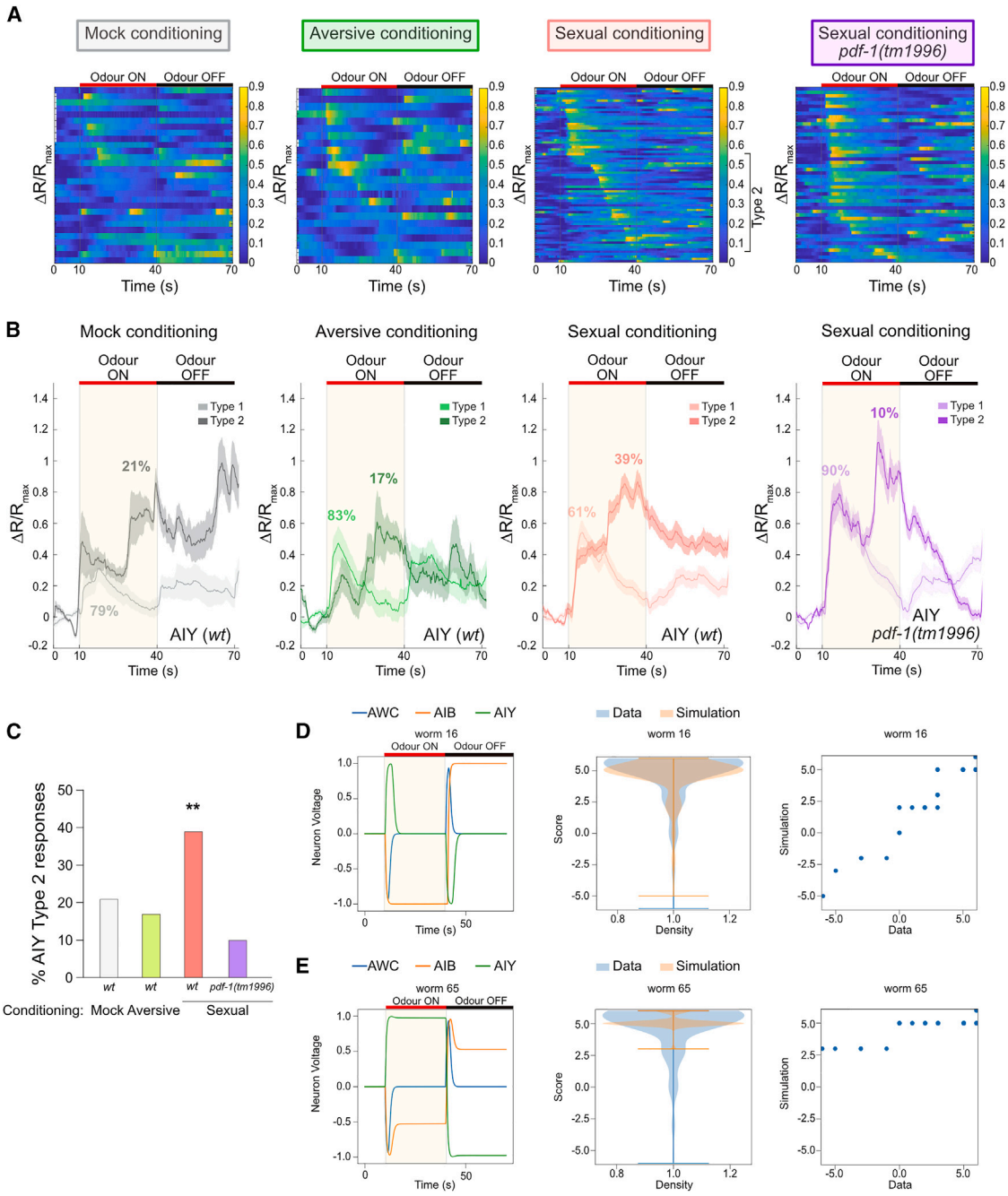

Figure 6. Sexual conditioning changes the neural representation of odor in AIY neurons in a PDF-1-dependent manner

(A) Odor-evoked normalized GCaMP6f/RFP fluorescence ratios in the axon of AIY after conditioning. Neurons are sorted according to time to maximum activation.

(B) Average normalized traces of type 1 and type 2 responses. Shaded areas represent SEM.

(C) Proportion of type 2 responses in AIY axons. χ^2 test was performed to compare between genotypes. $^{**}p < 0.01$.

(D) Simulated neural activity (left) and worm behavior (middle and right) of a population, with transient activity in AIY and sustained activity in AIB. Right, quantile-quantile (QQ) plot comparing the probability distribution of chemotaxis scores in the simulated and observed worm population.

(E) Same as (D) but for a population with sustained activity in AIY and reduced activity in AIB. For (D) and (E), bars within violin plots represent the 10th and 90th percentiles of each distribution.

See also Figures S4–S7.

behavioral data from mock-conditioned animals to fit the synaptic weights (the sign of the synapse was pre-set, according to functional connectivity) of a population of 100 simulated worms using an evolutionary algorithm over 100 generations (Figure S5). We then examined the simulated activity of AIY and AIB neurons in the final generation and their correlated chemotaxis scores (Figures S6–S8). Although none of the simulations fully recapitulated the real dynamics of activity in AIY and AIB, a good approximation of naive responses (transient AIY activity upon odor presentation and prolonged AIB activity after odor removal) was present in 20% of simulations. This neural activity was frequently correlated with attraction, with scores centered around +3 (Figures 6D, S6, and S7). Sustained AIY activity, approximating the type 2 responses observed in sexually conditioned animals, was produced in 45% of simulations, some of which (9%) were in the context of reduced AIB activity. For these, the chemotaxis scores shifted toward higher positive values, all above +3 and/or concentrated at +5 in 55% of the cases (Figures 6E, S6, and S7). Therefore, the simulations indicate that, in the context of reduced AIB activity, sustained AIY activity can lead to robust approach. Although it is likely that both aversive learning and sexual conditioning may create many other changes within the circuit for odor processing in addition to the ones identified in this work, our data show that distinct patterns of circuit activity underlie odor approach in naive versus sexually conditioned worms.

DISCUSSION

Specificity of information coding by neuropeptide signaling

Here, we have identified the mechanisms by which valence is flexibly modified by experience and neuropeptide signaling. We found that the neuropeptide PDF-1 can encode both positive and negative valence, depending on its neuronal sources and targets. PDF-1 release from the interneurons MCM and AVB provides information about mate experience, which acts as a teaching signal for reward. This signal is incorporated into the odor circuit through the interneurons RIM and RIA and modulation of odor-evoked Ca^{2+} responses in the axon of AIY. Underscoring the characteristic delay and slow kinetics with which neuropeptide signaling impacts neural circuit function and behavior, the source of PDF-1, AVB, becomes activated during conditioning but the consequences of PDF-1 neuromodulation on AIY are observed during retrieval. Modulation of this circuit by PDF-1 leads to odor approach. Detailed mapping of the circuit for avoidance awaits further study. The encoding of opposite valence by a single neuromodulator acting with circuit specificity appears to be a universal property of nervous systems.[48–53] It would be important to investigate the role that neuromodulation through mammalian vasoactive intestinal peptide (VIP), which belongs to the same family as PDF-1,[54,55] plays in associative learning, long-term potentiation, and memory retrieval in the cortex and amygdala.[56–59]

The mechanisms underlying sex-specific learning

As previously shown by Sakai et al., we find that mate experience is rewarding only for males because odor preferences can only be sexually conditioned in males. The neurons underlying sex-specific learning (AVB, RIM, RIA, and AIY), however, are present in both sexes. Although there is male-specific input connectivity from mate-sensing circuits into AVB, it remains unknown whether the other sex-shared neurons display dimorphism in their ability to respond to neuropeptide modulation to switch odor valence.

Although the male-specific MCM interneurons also receive input connectivity from mate-sensing circuits and are a required source of PDF-1, we did not observe changes in intracellular Ca^{2+} during conditioning. This suggests that other mechanisms may underlie their activation. A similar observation has been made for amphid single cilium I (ASI) neurons, which despite expressing receptors for pheromones and their function being required for pheromone-induced developmental and behavioral processes, do not display changes in intracellular Ca^{2+} levels upon pheromone exposure.[60–62] Alternative activation mechanisms may include changes in gene expression[63] or membrane excitability.[64] Nonetheless, we cannot rule out the possibility that our experimental system may not be sensitive enough to detect all meaningful Ca^{2+} changes.

Reward and punishment create two memories that co-exist and compete for behavioral expression

Our results reveal that pairing a stimulus with both a punishment and a reward creates two co-existing memories, one aversive and one rewarding, which compete for behavioral expression. The aversive memory, which arises from the association of an odor with the punishment of starvation and leads to odor avoidance, leaves a signature trace in the circuit characterized by reduced odor-evoked responses in AIB and RIM and nuclear translocation of EGL-4/PKG in AWC. This signature, which is absent in naive animals, remains present in animals that have been conditioned to associate the odor with both a punishment and the reward of mating partners (sexually conditioned animals) despite their behavior being approach. Reduction in AIB and RIM activity has only a small impact on behavior, and other unidentified changes, specifically those dependent on PDFR-1, are likely to contribute more strongly to full avoidance. Nonetheless, the changes in circuit activity that we observe after aversive conditioning represent the trace and storage of an aversive memory that remains latent after sexual conditioning. Indeed, memories can exist as biophysical and biochemical changes in the brain that are generated by previous experiences but that do not impact behavior.[65] These are latent memories, the behavioral expression of which is overridden by other memories such as, for example, extinction memories.[66]

Distinct neural representations of positive valence according to task functionality

Approach and avoidance are behavioral readouts of positive and negative valence, respectively. Research on how circuits encode valence has put forward two main functional types[67]: those that act as modules and those that act as modes. Modules are those in which approach and avoidance are encoded by the activity of distinct and segregated circuits.[52,53,68,69] Modes are those in which avoidance or approach are encoded by the activation or inhibition of a neuron (or circuit, brain region).[25,70,71] Here, we do not find evidence of either modules

CellPress
OPEN ACCESS

or modes. Instead, our results reveal that positive valence can be flexibly represented according to functionality or predictions associated with a stimulus. Although both naive and sexually conditioned animals display approach to the odor benzaldehyde, they display very different odor-evoked neural activity, and this likely reflects the different predictive value of the odor. Benzaldehyde, which is a bacterial metabolite, innately predicts food for naive animals. In sexually conditioned animals, in contrast, benzaldehyde predicts mates, and this is due to top-down modulation from downstream interneurons (AVB and MCM) to first-layer interneurons (AIY). A similar process of top-down modulation has been proposed for how sensory representation in the cortex changes according to task-specific brain states.[72] Here, we demonstrate that such flexible representation of sensory information can support learning and flexible behavior.

RESOURCE AVAILABILITY

Lead contact

Further information and requests for resources and reagents should be directed to and will be fulfilled by the lead contact, Arantza Barrios (a.barrios@ucl.ac.uk).

Materials availability

Plasmids and nematode strains generated in the course of this work are freely available to interested academic researchers through the lead contact.

Data and code availability

- Source data obtained in the current study have not been deposited in a public repository but are readily available from the lead contact upon request.
- All original code for the modeling has been deposited at https://github.com/ucl-cssb/worm_neural_nets/ and is publicly available. DOIs are listed in the key resources table.
- Any additional information required to reanalyze the data reported in this work is available from the lead contact upon request.

ACKNOWLEDGMENTS

We thank the following labs and individuals for strains and reagents: Bargmann (The Rockefeller University), L'Étoile (University of California, San Francisco), Carrera (Universidad de la Republica), Srinivasan (Worcester Polytechnic Institute), García (Texas A&M University), Hobert (Columbia University), Ch'ng (Kings' College London), Poole (UCL), Busch (Health and Medical University, Berlin), Temmerman (KU Leuven), Barkoulas (Imperial College London), Iino (University of Tokyo), Sengupta (Brandeis University), Rosie Truman (UCL), and Evie Goss-Sampson and Michele Sammut (UCL). Additional strains were obtained from the Caenorhabditis Genetic Center (University of Minnesota), which is supported by the National Institutes of Health – Office of Research Infrastructure Programs (P40 OD010440). We also thank Chintan Trivedi (UCL) for help in setting up the odor stimulation system. We are grateful to H. Buelow and our colleagues at UCL, J. Rihel, M. Amoyel, and V. Fernandes, for insightful comments on the manuscript. This work was supported by a Newton Fellowship from the Royal Society to L.M.-G. (NF160914), a Wellcome Trust PhD Studentship to S.C.-F. (175261), and a Leverhulme Trust project grant RPG-2022-066 to A.B.

AUTHOR CONTRIBUTIONS

A.B. conceived the project. A.B., L.M.-G., and S.C.-F. designed experiments, interpreted data, and co-wrote the manuscript. L.M.-G. and S.C.-F built the strains, performed the behavioral experiments and the neuronal recordings, and interpreted and analyzed the data. S.C.-F. developed custom MATLAB scripts to analyses the calcium imaging and behavior tracking data. E.C., L.L., S.B.-L., M.B., and B.G.-M.-O. contributed to imaging and behavioral experiments. N.J.T. and C.P.B. developed the computational model of odortaxis.

DECLARATION OF INTERESTS

The authors declare no competing interests.

STAR★METHODS

Detailed methods are provided in the online version of this paper and include the following:

- KEY RESOURCES TABLE
- EXPERIMENTAL MODEL AND STUDY PARTICIPANT DETAILS
- METHOD DETAILS
  - Odour conditioning assays
  - Plasmid constructs and transgenic strains
  - CaMPARI measurements
  - Calcium imaging
  - Microfluidic chip fabrication
  - Finite difference model of worm behaviour
- QUANTIFICATION AND STATISTICAL ANALYSIS
  - Calcium imaging analysis
  - Imaging of EGL-4 subcelluar localisation
  - Worm tracking
  - Statistical analysis

SUPPLEMENTAL INFORMATION

Supplemental information can be found online at https://doi.org/10.1016/j.cub.2024.10.024.

Received: April 10, 2023
Revised: June 18, 2024
Accepted: October 8, 2024
Published: November 14, 2024

REFERENCES

1. Dal Bello, M., Pérez-Escudero, A., Schroeder, F.C., and Gore, J. (2021). Inversion of pheromone preference optimizes foraging in C. elegans. eLife *10*, e58144.
2. Hughes, D.P., and Libersat, F. (2019). Parasite manipulation of host behavior. Curr. Biol. *29*, R45–R47.
3. Keleman, K., Vrontou, E., Krüttner, S., Yu, J.Y., Kurtovic-Kozaric, A., and Dickson, B.J. (2012). Dopamine neurons modulate pheromone responses in Drosophila courtship learning. Nature *489*, 145–149.
4. Zhang, Y., Lu, H., and Bargmann, C.I. (2005). Pathogenic bacteria induce aversive olfactory learning in Caenorhabditis elegans. Nature *438*, 179–184.
5. Ha, H.I., Hendricks, M., Shen, Y., Gabel, C.V., Fang-Yen, C., Qin, Y., Colón-Ramos, D., Shen, K., Samuel, A.D.T., and Zhang, Y. (2010). Functional organization of a neural network for aversive olfactory learning in Caenorhabditis elegans. Neuron *68*, 1173–1186.
6. Li, Q., and Liberles, S.D. (2015). Aversion and attraction through olfaction. Curr. Biol. *25*, R120–R129.
7. Tye, K.M. (2018). Neural circuit motifs in valence processing. Neuron *100*, 436–452.
8. Wagle, M., Zarei, M., Lovett-Barron, M., Poston, K.T., Xu, J., Ramey, V., Pollard, K.S., Prober, D.A., Schulkin, J., Deisseroth, K., et al. (2022). Brain-wide perception of the emotional valence of light is regulated by distinct hypothalamic neurons. Mol. Psychiatry *27*, 3777–3793.
9. Carew, T.J., Walters, E.T., and Kandel, E.R. (1981). Classical conditioning in a simple withdrawal reflex in Aplysia californica. J. Neurosci. *1*, 1426–1437.

10. Ward, S. (1973). Chemotaxis by the nematode Caenorhabditis elegans: identification of attractants and analysis of the response by use of mutants. Proc. Natl. Acad. Sci. USA *70*, 817–821.
11. Bargmann, C.I., Hartwieg, E., and Horvitz, H.R. (1993). Odorant-selective genes and neurons mediate olfaction in C. elegans. Cell *74*, 515–527.
12. Tomioka, M., Adachi, T., Suzuki, H., Kunitomo, H., Schafer, W.R., and Iino, Y. (2006). The insulin/PI 3-kinase pathway regulates salt chemotaxis learning in Caenorhabditis elegans. Neuron *51*, 613–625.
13. Nuttley, W.M., Atkinson-Leadbeater, K.P., and Van Der Kooy, D. (2002). Serotonin mediates food-odor associative learning in the nematode Caenorhabditiselegans. Proc. Natl. Acad. Sci. USA *99*, 12449–12454.
14. Lin, C.H.A., Tomioka, M., Pereira, S., Sellings, L., Iino, Y., and van der Kooy, D. (2010). Insulin signaling plays a dual role in Caenorhabditis elegans memory acquisition and memory retrieval. J. Neurosci. *30*, 8001–8011.
15. Sakai, N., Iwata, R., Yokoi, S., Butcher, R.A., Clardy, J., Tomioka, M., and Iino, Y. (2013). A sexually conditioned switch of chemosensory behavior in C. elegans. PLoS One *8*, e68676.
16. Sammut, M., Cook, S.J., Nguyen, K.C.Q., Felton, T., Hall, D.H., Emmons, S.W., Poole, R.J., and Barrios, A. (2015). Glia-derived neurons are required for sex-specific learning in C. elegans. Nature *526*, 385–390.
17. Barrios, A., Nurrish, S., and Emmons, S.W. (2008). Sensory regulation of C. elegans male mate-searching behavior. Curr. Biol. *18*, 1865–1871.
18. Lipton, J., Kleemann, G., Ghosh, R., Lints, R., and Emmons, S.W. (2004). Mate searching in Caenorhabditis elegans: a genetic model for sex drive in a simple invertebrate. J. Neurosci. *24*, 7427–7434.
19. Janssen, T., Husson, S.J., Lindemans, M., Mertens, I., Rademakers, S., Ver Donck, K., Geysen, J., Jansen, G., and Schoofs, L. (2008). Functional characterization of three G protein-coupled receptors for pigment dispersing factors in Caenorhabditis elegans. J. Biol. Chem. *283*, 15241–15249.
20. Janssen, T., Husson, S.J., Meelkop, E., Temmerman, L., Lindemans, M., Verstraelen, K., Rademakers, S., Mertens, I., Nitabach, M., Jansen, G., et al. (2009). Discovery and characterization of a conserved pigment dispersing factor-like neuropeptide pathway in Caenorhabditis elegans. J. Neurochem. *111*, 228–241.
21. Barrios, A., Ghosh, R., Fang, C., Emmons, S.W., and Barr, M.M. (2012). PDF-1 neuropeptide signaling modulates a neural circuit for mate-searching behavior in C. elegans. Nat. Neurosci. *15*, 1675–1682.
22. Flavell, S.W., Pokala, N., Macosko, E.Z., Albrecht, D.R., Larsch, J., and Bargmann, C.I. (2013). Serotonin and the neuropeptide PDF initiate and extend opposing behavioral states in C. elegans. Cell *154*, 1023–1035.
23. Chalasani, S.H., Chronis, N., Tsunozaki, M., Gray, J.M., Ramot, D., Goodman, M.B., and Bargmann, C.I. (2007). Dissecting a circuit for olfactory behaviour in Caenorhabditis elegans. Nature *450*, 63–70.
24. Gordus, A., Pokala, N., Levy, S., Flavell, S.W., and Bargmann, C.I. (2015). Feedback from network states generates variability in a probabilistic olfactory circuit. Cell *161*, 215–227.
25. Guillermin, M.L., Carrillo, M.A., and Hallem, E.A. (2017). A single set of interneurons drives opposite behaviors in C. elegans. Curr. Biol. *27*, 2630–2639.e6.
26. Jin, X., Pokala, N., and Bargmann, C.I. (2016). Distinct circuits for the formation and retrieval of an imprinted olfactory memory. Cell *164*, 632–643.
27. Brockie, P.J., Madsen, D.M., Zheng, Y., Mellem, J., and Maricq, A.V. (2001). Differential expression of glutamate receptor subunits in the nervous system of Caenorhabditis elegans and their regulation by the homeodomain protein UNC-42. J. Neurosci. *21*, 1510–1522.
28. Hobert, O., Mori, I., Yamashita, Y., Honda, H., Ohshima, Y., Liu, Y., and Ruvkun, G. (1997). Regulation of interneuron function in the C. elegans thermoregulatory pathway by the ttx-3 LIM homeobox gene. Neuron *19*, 345–357.
29. Pokala, N., Liu, Q., Gordus, A., and Bargmann, C.I. (2014). Inducible and titratable silencing of Caenorhabditis elegans neurons in vivo with histamine-gated chloride channels. Proc. Natl. Acad. Sci. USA *111*, 2770–2775.
30. Cook, S.J., Jarrell, T.A., Brittin, C.A., Wang, Y., Bloniarz, A.E., Yakovlev, M.A., Nguyen, K.C.Q., Tang, L.T.H., Bayer, E.A., Duerr, J.S., et al. (2019). Whole-animal connectomes of both Caenorhabditis elegans sexes. Nature *571*, 63–71.
31. Srinivasan, J., Kaplan, F., Ajredini, R., Zachariah, C., Alborn, H.T., Teal, P.E.A., Malik, R.U., Edison, A.S., Sternberg, P.W., and Schroeder, F.C. (2008). A blend of small molecules regulates both mating and development in Caenorhabditis elegans. Nature *454*, 1115–1118.
32. Liu, K.S., and Sternberg, P.W. (1995). Sensory regulation of male mating behavior in Caenorhabditis elegans. Neuron *14*, 79–89.
33. Barr, M.M., and Sternberg, P.W. (1999). A polycystic kidney-disease gene homologue required for male mating behaviour in C. elegans. Nature *401*, 386–389.
34. Fosque, B.F., Sun, Y., Dana, H., Yang, C.T., Ohyama, T., Tadross, M.R., Patel, R., Zlatic, M., Kim, D.S., Ahrens, M.B., et al. (2015). Neural circuits. Labeling of active neural circuits in vivo with designed calcium integrators. Science *347*, 755–760.
35. Kato, S., Kaplan, H.S., Schrödel, T., Skora, S., Lindsay, T.H., Yemini, E., Lockery, S., and Zimmer, M. (2015). Global brain dynamics embed the motor command sequence of Caenorhabditis elegans. Cell *163*, 656–669.
36. Atanas, A.A., Kim, J., Wang, Z., Bueno, E., Becker, M., Kang, D., Park, J., Kramer, T.S., Wan, F.K., Baskoylu, S., et al. (2023). Brain-wide representations of behavior spanning multiple timescales and states in C. elegans. Cell *186*, 4134–4151.e31.
37. Chronis, N., Zimmer, M., and Bargmann, C.I. (2007). Microfluidics for in vivo imaging of neuronal and behavioral activity in Caenorhabditis elegans. Nat. Methods *4*, 727–731.
38. Reilly, D.K., Lawler, D.E., Albrecht, D.R., and Srinivasan, J. (2017). Using an adapted microfluidic olfactory chip for the imaging of neuronal activity in response to pheromones in male C. elegans Head neurons. J. Vis. Exp.
39. Chalasani, S.H., Kato, S., Albrecht, D.R., Nakagawa, T., Abbott, L.F., and Bargmann, C.I. (2010). Neuropeptide feedback modifies odor-evoked dynamics in Caenorhabditis elegans olfactory neurons. Nat. Neurosci. *13*, 615–621.
40. Liu, H., Yang, W., Wu, T., Duan, F., Soucy, E., Jin, X., and Zhang, Y. (2018). Cholinergic sensorimotor integration regulates olfactory steering. Neuron *97*, 390–405.e3.
41. Gray, J.M., Hill, J.J., and Bargmann, C.I. (2005). A circuit for navigation in Caenorhabditis elegans. Proc. Natl. Acad. Sci. USA *102*, 3184–3191.
42. Flavell, S.W., Raizen, D.M., and You, Y.J. (2020). Behavioral states. Genetics *216*, 315–332.
43. Barrios, A. (2014). Exploratory decisions of the Caenorhabditis elegans male: a conflict of two drives. Semin. Cell Dev. Biol. *33*, 10–17.
44. Lee, J.I., O'Halloran, D.M., Eastham-Anderson, J., Juang, B.T., Kaye, J.A., Scott Hamilton, O., Lesch, B., Goga, A., and L'Etoile, N.D. (2010). Nuclear entry of a cGMP-dependent kinase converts transient into long-lasting olfactory adaptation. Proc. Natl. Acad. Sci. USA *107*, 6016–6021.
45. Cho, C.E., Brueggemann, C., L'Etoile, N.D., and Bargmann, C.I. (2016). Parallel encoding of sensory history and behavioral preference during Caenorhabditis elegans olfactory learning. eLife *5*, e14000.
46. Tsalik, E.L., and Hobert, O. (2003). Functional mapping of neurons that control locomotory behavior in Caenorhabditis elegans. J. Neurobiol. *56*, 178–197.
47. Ben Arous, J., Laffont, S., and Chatenay, D. (2009). Molecular and sensory basis of a food related two-state behavior in C. elegans. PLoS One *4*, e7584.
48. Cohn, R., Morantte, I., and Ruta, V. (2015). Coordinated and compartmentalized neuromodulation shapes sensory processing in Drosophila. Cell *163*, 1742–1755.
49. Traniello, I.M., Chen, Z., Bagchi, V.A., and Robinson, G.E. (2019). Valence of social information is encoded in different subpopulations of mushroom body Kenyon cells in the honeybee brain. Proc. Biol. Sci. *286*, 20190901.

50. de Jong, J.W., Afjei, S.A., Pollak Dorocic, I., Peck, J.R., Liu, C., Kim, C.K., Tian, L., Deisseroth, K., and Lammel, S. (2019). A neural circuit mechanism for encoding aversive stimuli in the mesolimbic dopamine system. Neuron *101*, 133–151.e7.

51. McGovern, D.J., Polter, A.M., and Root, D.H. (2021). Neurochemical signaling of reward and aversion to ventral tegmental area glutamate neurons. J. Neurosci. *41*, 5471–5486.

52. Li, H., Namburi, P., Olson, J.M., Borio, M., Lemieux, M.E., Beyeler, A., Calhoon, G.G., Hitora-Imamura, N., Coley, A.A., Libster, A., et al. (2022). Neurotensin orchestrates valence assignment in the amygdala. Nature *608*, 586–592.

53. Zhang, X., Guan, W., Yang, T., Furlan, A., Xiao, X., Yu, K., An, X., Galbavy, W., Ramakrishnan, C., Deisseroth, K., et al. (2021). Genetically identified amygdala-striatal circuits for valence-specific behaviors. Nat. Neurosci. *24*, 1586–1600.

54. Frooninckx, L., Van Rompay, L., Temmerman, L., Van Sinay, E., Beets, I., Janssen, T., Husson, S.J., and Schoofs, L. (2012). Neuropeptide GPCRs in C. elegans. Front. Endocrinol. (Lausanne) *3*, 167.

55. Janssen, T., Lindemans, M., Meelkop, E., Temmerman, L., and Schoofs, L. (2010). Coevolution of neuropeptidergic signaling systems: from worm to man. Ann. N. Y. Acad. Sci. *1200*, 1–14.

56. Pi, H.J., Hangya, B., Kvitsiani, D., Sanders, J.I., Huang, Z.J., and Kepecs, A. (2013). Cortical interneurons that specialize in disinhibitory control. Nature *503*, 521–524.

57. Krabbe, S., Paradiso, E., d'Aquin, S., Bitterman, Y., Courtin, J., Xu, C., Yonehara, K., Markovic, M., Müller, C., Eichlisberger, T., et al. (2019). Adaptive disinhibitory gating by VIP interneurons permits associative learning. Nat. Neurosci. *22*, 1834–1843.

58. Melzer, S., Newmark, E.R., Mizuno, G.O., Hyun, M., Philson, A.C., Quiroli, E., Righetti, B., Gregory, M.R., Huang, K.W., Levasseur, J., et al. (2021). Bombesin-like peptide recruits disinhibitory cortical circuits and enhances fear memories. Cell *184*, 5622–5634.e25.

59. Williams, L.E., and Holtmaat, A. (2019). Higher-order thalamocortical inputs gate synaptic long-term potentiation via disinhibition. Neuron *101*, 91–102.e4.

60. Kim, K., Sato, K., Shibuya, M., Zeiger, D.M., Butcher, R.A., Ragains, J.R., Clardy, J., Touhara, K., and Sengupta, P. (2009). Two chemoreceptors mediate developmental effects of dauer pheromone in C. elegans. Science *326*, 994–998.

61. Luo, J., and Portman, D.S. (2021). Sex-specific, pdfr-1-dependent modulation of pheromone avoidance by food abundance enables flexibility in C. elegans foraging behavior. Curr. Biol. *31*, 4449–4461.e4.

62. McGrath, P.T., Xu, Y., Ailion, M., Garrison, J.L., Butcher, R.A., and Bargmann, C.I. (2011). Parallel evolution of domesticated Caenorhabditis species targets pheromone receptor genes. Nature *477*, 321–325.

63. Laurent, P., Soltesz, Z., Nelson, G.M., Chen, C., Arellano-Carbajal, F., Levy, E., and de Bono, M. (2015). Decoding a neural circuit controlling global animal state in C. elegans. eLife *4*, e04241.

64. Stout, R.F., Jr., Verkhratsky, A., and Parpura, V. (2014). Caenorhabditis elegans glia modulate neuronal activity and behavior. Front. Cell. Neurosci. *8*, 67.

65. Josselyn, S.A., and Tonegawa, S. (2020). Memory engrams: recalling the past and imagining the future. Science *367*, eaaw4325.

66. Felsenberg, J., Jacob, P.F., Walker, T., Barnstedt, O., Edmondson-Stait, A.J., Pleijzier, M.W., Otto, N., Schlegel, P., Sharifi, N., Perisse, E., et al. (2018). Integration of parallel opposing memories underlies memory extinction. Cell *175*, 709–722.e15.

67. Berridge, K.C. (2019). Affective valence in the brain: modules or modes? Nat. Rev. Neurosci. *20*, 225–234.

68. Li, Y., Li, C.Y., Xi, W., Jin, S., Wu, Z.H., Jiang, P., Dong, P., He, X.B., Xu, F.Q., Duan, S., et al. (2019). Rostral and caudal ventral tegmental area GABAergic inputs to different dorsal raphe neurons participate in opioid dependence. Neuron *101*, 748–761.e745.

69. Waddell, S. (2013). Reinforcement signalling in Drosophila; dopamine does it all after all. Curr. Opin. Neurobiol. *23*, 324–329.

70. Pirger, Z., László, Z., Naskar, S., Crossley, M., O'Shea, M., Benjamin, P.R., Kemenes, G., and Kemenes, I. (2021). Interneuronal mechanisms for learning-induced switch in a sensory response that anticipates changes in behavioral outcomes. Curr. Biol. *31*, 1754–1761.e3.

71. Fagan, K.A., Luo, J., Lagoy, R.C., Schroeder, F.C., Albrecht, D.R., and Portman, D.S. (2018). A single-neuron chemosensory switch determines the valence of a sexually dimorphic sensory behavior. Curr. Biol. *28*, 902–914.e5.

72. Zhang, N., and Xu, N.L. (2022). Reshaping sensory representations by task-specific brain states: toward cortical circuit mechanisms. Curr. Opin. Neurobiol. *77*, 102628.

73. Javer, A., Ripoll-Sánchez, L., and Brown, A.E.X. (2018). Powerful and interpretable behavioural features for quantitative phenotyping of Caenorhabditis elegans. Philos. Trans. R. Soc. Lond. B Biol. Sci. *373*, 20170375.

74. Brenner, S. (1974). The genetics of *Caenorhabditis elegans*. Genetics *77*, 71–94.

75. Stiernagle, T. (2006). Maintenance of C. elegans. WormBook, 1–11.

76. Gibson, D.G., Young, L., Chuang, R.Y., Venter, J.C., Hutchison, C.A., and Smith, H.O. (2009). Enzymatic assembly of DNA molecules up to several hundred kilobases. Nat. Methods *6*, 343–345.

77. Gibson, D.G., Glass, J.I., Lartigue, C., Noskov, V.N., Chuang, R.Y., Algire, M.A., Benders, G.A., Montague, M.G., Ma, L., Moodie, M.M., et al. (2010). Creation of a bacterial cell controlled by a chemically synthesized genome. Science *329*, 52–56.

78. Mello, C.C., Kramer, J.M., Stinchcomb, D., and Ambros, V. (1991). Efficient gene transfer in C.elegans: extrachromosomal maintenance and integration of transforming sequences. EMBO J. *10*, 3959–3970.

79. Berkowitz, L.A., Knight, A.L., Caldwell, G.A., and Caldwell, K.A. (2008). Generation of stable transgenic C. elegans using microinjection. J. Vis. Exp.

80. Kim, E., Sun, L., Gabel, C.V., and Fang-Yen, C. (2013). Long-term imaging of Caenorhabditis elegans using nanoparticle-mediated immobilization. PLoS One *8*, e53419.

81. Lagoy, R.C., and Albrecht, D.R. (2015). Microfluidic devices for behavioral analysis, microscopy, and neuronal imaging in Caenorhabditis elegans. Methods Mol. Biol. *1327*, 159–179.

82. Ghosh, D.D., Sanders, T., Hong, S., McCurdy, L.Y., Chase, D.L., Cohen, N., Koelle, M.R., and Nitabach, M.N. (2016). Neural architecture of hunger-dependent multisensory decision making in C. elegans. Neuron *92*, 1049–1062.

83. Busch, K.E., Laurent, P., Soltesz, Z., Murphy, R.J., Faivre, O., Hedwig, B., Thomas, M., Smith, H.L., and de Bono, M. (2012). Tonic signaling from O(2) sensors sets neural circuit activity and behavioral state. Nat. Neurosci. *15*, 581–591.

84. Kaplan, H.S., Salazar Thula, O., Khoss, N., and Zimmer, M. (2020). Nested neuronal dynamics orchestrate a behavioral hierarchy across timescales. Neuron *105*, 562–576.e9.

STAR★METHODS

KEY RESOURCES TABLE

REAGENT or RESOURCE	SOURCE	IDENTIFIER
Bacterial and virus strains		
Escherichia coli OP50	Caenorhabditis Genetic Center (CGC)	OP50
Chemicals, peptides, and recombinant proteins		
Benzaldehyde	Sigma-Aldrich	Cat#B-1334
Butanone	Scientific Laboratory Supplies (SLS)	Cat#CHE1442
Histamine	Sigma-Aldrich	Cat#H7125
SYLGARD™ 184 Silicone Elastomer Kit	Scientific Laboratory Supplies (SLS)	Cat#63416.5S
Tetramisole hydrochloride phosphatase inhibitor	Sigma-Aldrich	Cat#T1512
Fluorescein isothiocyanate-dextran	Sigma-Aldrich	Cat#FD2000S
Critical commercial assays		
Monarch Plasmid Miniprep Kit	New England Biolabs	Cat#T1010L
NEBuilder HiFi DNA Assembly Master Mix	New England Biolabs	Cat#E2621L
Monarch PCR & DNA clean kit	New England Biolabs	Cat#T1030L
Q5 High Fidelity DNA polymerase	New England Biolabs	Cat#M0491L
PCRBIO Hi-Fi Polymerase	Insight Biotechnology (PCR Biosystems)	Cat#PB10.41-02
Deposited data		
Modelling Code	This work	https://github.com/ucl-cssb/worm_neural_nets/
Experimental models: Organisms/strains		
N2 Bristol	CGC	N2
him-5(e1490)V	CGC	CB4088
*pdf-1(tm1996)*III; *him-5(e1490)*V	This work/Barrios et al.[21]	BAR109/ PT2248
pdf-2(tm4393) X; *him-5 (e1490)* V	Barrios et al.[21]	PT2177
*pdf-2(tm4393)*X; *pdf-1(tm1996)*III;*him-5(e1490)*V	Barrios et al.[21]	PT2159
*him-5 (e1490)*V; *pdf-1(tm1996)*III; *syb1393[AB01(pLAU-1-EG6699)MosCi LoxP::pdf-1cDNA::SL2::gfp::loxP::rfp]*II	This work	BAR155
him-5 (e1490) V; *pdf-1(tm1996)*III; *syb1393* II; *oleEx39[grl-2::Cre+cc::rfp]*	This work	BAR167
him-5 (e1490) V; *pdf-1(tm1996)*III;*syb1393* II;*kyEx4983 [sra-11::nCre(35ng/uL), myo-3::mCherry (5ng/uL)]*	This work	BAR169
him-5 (e1490) V; *pdf-1(tm1996)*III;*syb1393* II;*kyEx4990[ceh-17::nCre(40ng/uL), myo-3::mCherry(5ng/uL)]*	This work	BAR170
*pdf-2(tm4393)*X;*pdf-1(tm1996)*III;*him-5(e1490)*V;*syb1393* II	This work	BAR187
*pdf-2(tm4393)*X;*pdf-1(tm1996)*III;*him-5(e1490)*V;*syb1393* II; *oleEx39[grl-2(p)::Cre(30ng/μl)+cc::RFP(30ng/μl)]*	This work	BAR188
*pdf-2(tm4393)*X;*pdf-1(tm1996)*III;*him-5(e1490)*V; *syb1393* II; *kyEx4983[sra-11::nCre (35ng/ul), myo-3::mCherry (5ng/ul)]*	This work	BAR189
*pyIs500[(p)odr-3::gfp::egl-4+(p)odr-1::dsRed1+unc-122::GFP]*V;*him-5(e1490)*V	Lee et al.[44]/This work	BAR108
*him-5(e1490)*V; *oleEx80 [ttx-3::GCaMP6f::sl2::rfp (5ng/uL)]*	This work	BAR224
*him-5(e1490)*V; *pdf-1(tm1996)*III; *oleEx80 [ttx-3::GCaMP6f::sl2::rfp (5ng/uL)]*	This work	BAR227

(*Continued on next page*)

Continued

REAGENT or RESOURCE	SOURCE	IDENTIFIER
him-5(e1490)V;oleEx64[inx-1::GCaMP6f::sl2::rfp (15ng/ul)+ ttx-3::GCaMP6f::sl2::rfp (15ng/uL)]	This work	BAR184
him-5(e1490)V; oleEx103[glr-3::GCaMP6f::sl2::rfp (30ng/uL)]	This work	BAR269
him-5(e1490)V;oleEx95[tdc-1::GCaMP6f::sl2::rfp (10ng/uL)]	This work	BAR253
pdfr-1(tm4457)III;him-5(e1490)V;myEx709[Ppdfr-1(3kb)::pdfr-1cDNAisofb+Ppdfr-1(3kb)::pdfr-1cDNAisofd+unc-122::GFP]	This work	BAR122
pdfr-1(tm4457)III; him-5(e1490)V; oleIs3[pdfr-1::LoxP::inv pdfr-1cDNAisofD::sl2::GFP::LoxP(10ng/μl)+ unc122::GFP(10ng/μl)]; oleIs5[rab-3::nCre (3ng/ul)+unc-122::RFP (30 ng/ul)]	This work	BAR273
pdfr-1(tm4457)III; him-5(e1490)V; oleIs3	This work	BAR176
pdfr1(tm4457)III; him-5(e1490)V; oleIs 3; oleEx72[tdc-1::nCre (20 ng/uL pSF178)+ glr-3::nCre (50 ng/uL pSF179) + ttx-3::nCre (5 ng/uL pLAU 11)+ unc122::RFP(25ng/uL)]	This work	BAR206
pdfr-1(tm4457)III; him-5(e1490)V	Barrios et al.[21]	PT2547
lite-1(ce314)X;him-5(e1490)V;oleEx58[pdf-1:: Campari (25 ng/μl) + cc::GFP (30ng/μl)]	This work	BAR196
pdf-1(tm1996)III;him-5(e1490)V; oleEx39[grl-2(p)::Cre(30ng/μl)+cc::RFP(30ng/μl)]	This work	BAR119
unc-51(e369)	CGC	CB369
pdfr-1(tm4457)III; him-5(e1490)V;oleIs5	This work	BAR215
him-5(e1490); oleEx110[glr3::HisCl (50ng/uL); tdc-1::HisCl (20ng/uL); ttx-3::HisCl (5 ng/uL); unc-122::RFP (15 ng/ul)]	This work	BAR294
him-5 (e1490) V; kyEx5704 [inx-1::HisCl1::SL2::mCherry 50 ng/mL, tdc-1::HisCl1::SL2::mCherry 50 ng/mL]	This work	BAR302
mab-3 (e1240)II;him-5(e1490)V; oleEx58[pdf-1::Campari (25 ng/μl) + cc::GFP (30ng/μl)]	This work	BAR320
Oligonucleotides		
See Table S2		
Recombinant DNA		
Mos ttTi5605-pdf-1::lox pdf-1-sl2-GFPlox RFP unc-119 MosttTi560	This work	pLAU-1
grl-2::nCre	This work	pLAU-2
rab-3::nCre	This work	pLAU-4
glr-3::GCAMP6f-sl2-RFP	This work	pLAU-9
tdc-1::GCAMP6f-sl2-RFP	This work	pLAU-10
ttx-3::nCre	This work	pLAU-11
pdfr-1 distal floxed pdfr-1 iso d	Flavell et al.[42]	pSF134
pdf-1::lox pdf-1-sl2-GFPlox RFP	Flavell et al.[42]	pSF153
tdc-1::nCre	Flavell et al.[42]	pSF178
glr-3::nCre	Flavell et al.[42]	pSF179
ncs-1::nCre	Addgene	pEM3
pdf-1::CAMPARI	This work	pRTAB1
inx-1::GCaMP6f-sl2-RFP	This work	pAB1
ttx-3::GCaMP6f-sl2-RFP	This work	pAB2
Mos ttTi5605 -unc-119- MosttTi5605	Queelim Ch'ng Lab	pQL123
tdc-1::HisCl-sl2-mCherry	Jin et al.[26]	pAG04
glr-3::HisCl-sl2-mCherry	Jin et al.[26]	pNP443
ttx-3::HisCl-sl2-mCherry	Jin et al.[26]	pNP501

(*Continued on next page*)

Continued

REAGENT or RESOURCE	SOURCE	IDENTIFIER
Software and algorithms		
GraphPad Prism	GraphPad Prism (http://graphpad.com)	RRID:SCR_002798
Image J	ImageJ (http://imagej.nih.gov/ij/)	RRID:SCR_003070
Motif Video Recording system	http://loopbio.com/recording/	Loopbio
Time ToLIve	http://www.simi.com/	Caenotec
Arduino IDE	https://www.arduino.cc/en/software	Version 1.8.13
Tierpsy	Javer et al.[73]	https://github.com/Tierpsy/tierpsy-tracker
HC Image live	Hamamatsu	N/A
NEB Builder Assembly Tool	NEB (https://nebuilder.neb.com/#!/)	N/A
QMPlay2	GitHub https://appimage.github.io/QMPlay2/	N/A
Other		
Arduino Board	https://store.arduino.cc/products/arduino-uno-rev3	Arduino UNO R3

EXPERIMENTAL MODEL AND STUDY PARTICIPANT DETAILS

C. elegans culture and genetics were performed using *Escherichia coli* OP50 and NGM plates following standard procedures.[74,75] A complete list of the strains used can be found in the key resources table. All strains were in a *him-5* (e1490) background to facilitate male analysis, except for Figure 1B for which *him-8(e1489)* animals were used. Unless stated otherwise, all strains were grown and assayed at 20ºC.

METHOD DETAILS

Odour conditioning assays

Males and hermaphrodites were picked as L4s the night before the assay and transferred to single-sex plates with food. Animals were recovered from the food plates with wash buffer (1 mM $CaCl_2$, 1 mM $MgSO_4$, and 5 mM pH 6.0 potassium phosphate) and centrifuged at 1,700 r.p.m. for 3 min. A total of four washes were performed to remove the food before placing the animals on the conditioning plates.

Odour conditioning assay plates were made with 2% agar, 5 mM potassium phosphate (pH 6.0), 1 mM $CaCl_2$ and 1 mM $MgSO_4$. Mock conditioning plates were 5 cm in diameter (4 ml of agar), whereas aversive and sexual conditioning plates were 3 cm in diameter (2 ml of agar). Between 20–30 males were placed on each mock and aversive conditioning plate and exposed to either 100% ethanol or 15% benzaldehyde, respectively. For sexual conditioning, a maximum of 30 males and 200 hermaphrodites were used and animals were exposed to 15% benzaldehyde. Genotypes that were being compared against one another were sexually conditioned together in the same plate, tested and scored blindly and then identified through genotyping or by fluorescent markers. When different genotypes were conditioned together equal amounts of each genotype were used until a total of 30 males were added to the sexual conditioning plate. Controls in which animals were exposed to the odour on food were also performed for some experiments. In all cases animals were conditioned for 3 h. Immediately after conditioning, animals were tested individually in 5 cm plates with a 1% benzaldehyde gradient by placing them in the centre of the assay plate, 2 cm away from the odour source (Figure 1A). After 20 min, the tracks left by the animal were visualised and the chemotaxis score was calculated as previously described[15] by the sum of the scores of the regions by which the animal had travelled (Figure 1A). Scoring of all sexual conditioning experiments were blind to the manipulation.

For butanone behaviour assays, 1:1000 butanone in ethanol was used for conditioning (5 x 1μL on agar plugs on lid), and testing (1x1μL directly on plate agar).

For histamine-treated behaviour assays, histamine was added to the agar before pouring to a final concentration of 10mM. Worms were conditioned on histamine plates for 3h and tested on standard chemotaxis plates.

unc-51(e369) hermaphrodites were used for sexual conditioning in the calcium imaging experiments and behaviour experiments with histamine and *mab-3(e1240)* mutants. All other sexual conditioning behavioural experiments were performed using N2 hermaphrodites.

Plasmid constructs and transgenic strains

All constructs were built using Gibson Assembly.[76,77] Primers were designed using the NEBuilder assembly online tool (https://nebuilder.neb.com). The 3′ UTR of the *unc-54* gene was used for all constructs. Two different promoters were used to express

pdfr-1 in different cells. A promoter containing a 3kb region upstream of the translational *pdfr-1* start site (proximal promoter) drove *pdfr-1* isoforms b and d in neurons and body wall muscle[21] (Figure 2B). A second construct drove a floxed isoform d in reverse orientation under a 5.1 kb sequence located 12.1Kb upstream of the translational *pdfr-1* start site (distal promoter)[22] (Figure 2B). This construct was used to express *pdfr-1* cDNA isoform d in specific neurons through intersectional expression of Cre recombinase (Figure 2B) A complete list of primers and plasmids used in this study can be found in Table S2 and key resources table, respectively. Plasmid constructs were injected in *C. elegans* following standard procedures.[78,79] The specific co-injection marker used as well as the concentration at which each array was injected can be found in key resources table.

CaMPARI measurements

*lite-1(ce314)*X; *him-5(e1490)*V; *oleEx58[pdf-1::Campari (25 ng/μl) + cc::GFP (30ng/μl)]* males were conditioned with 15% benzaldehyde in 3 cm plates with no food and with or without *unc-51* hermaphrodites for sexual and aversive conditioning, respectively. At 3 hrs during conditioning, CaMPARI was photoconverted by exposing the conditioning plates to 405nm blue light (DAPI filter) for 2 minutes at 50% LED intensity under an inverted Zeiss Axiovert microscope and a 10x objective. Images of the MCM and AVB neurons were taken by mounting worms in 10% agarose pads with undiluted microbeads.[80] Classically used anesthetics such as NaN_3 or levamisole could not be used because they interfere with the fluorescence signal of CaMPARI. Photos were taken with a Zeiss Axio Imager 2 microscope using a 470nm LED source at 25% intensity and EX470/20 FT493 EM505-503 filter for the green channel and GYR LED source at 50% intensity and BP546/12 FT580 LP590 filter for the red channel and at 125x magnification. LED intensity and exposure time were kept constant for AVB and MCM neurons across the sample population but longer exposure was needed for the MCM neurons. Experiments with *mab-3* mutants (along with wild type males as positive controls) were performed on a different day and with exposure times distinct from previous experiments.

Image analysis was performed using Fiji. Before image processing, background intensity was subtracted from both channels. The average fluorescence intensity for each channel was measured by manually drawing a polygon containing the region of interest (ROI) on the z-plane at which the neuron analysed provided the brightest signal. The ratio between the average fluorescence intensity for green and red channels was calculated for each ROI.

Calcium imaging

Animals were first subjected to one of the three conditioning protocols in the same way as for behavioural analysis. Immediately after conditioning, animals were injected into a nose trap microfluidic device[37] using wash buffer 1 mM $CaCl_2$, 1 mM $MgSO_4$, and 5 mM pH 6.0 potassium phosphate and 0.5 mM tetramisole to reduce movement of the animals while imaging. Animals were exposed to alternative periods of 10^{-4} benzaldehyde (diluted in wash buffer, no fluorescein) or wash buffer with 0.003 mg/ml fluorescein. Flow control buffer contained 0.03 mg/ml fluorescein. This allowed visualisation of flow with fluorescence, and control checks of adequate flow were done between every recording. Imaging was performed in an inverted Zeiss Axiovert microscope with a 460/565nm LED. Emission filters ET515/30M and ET641/75 and dichroic T565lprx-UF2 were placed in the cube of a Cairn OptoSplit II attached between the microscope and an ORCA-Flash four camera (Hamamatsu). Acquisition was performed at 10 fps with a 63X objective (Zeiss plan-apochromat, numerical aperture 1.4) and 1.5X optovar, using HC image live from Hamamatsu. To avoid photobleaching pulse illumination was used. The cell body was imaged for AIB neurons, whereas the projection was imaged for RIM, AIY (specifically zone 2), and RIA (loop domain, ventral nerve ring domain and dorsal nerve ring domain).

Microfluidic chip fabrication

Male-adapted polydimethylsiloxane (PDMS) olfactory chips[38] were made and plasma-bonded to a glass coverslip as previously described.[38,81] After plasma bonding, chips were placed on a hot plate at 80 ºC for one hour to improve bonding efficiency.

Finite difference model of worm behaviour

To investigate the worm's behaviour an ordinary differential equation model was developed (Figure S4). This simulated the worm's response to a concentration gradient by modelling a simple neural network. The network was comprised of the AWC sensory neurons and the AIB, AIA and AIY neurons. We adapted the modelling approach in.[82] The sensory neuron AWC is comprised of two components which react to the concentration of odour on different timescales, a fast, F, and slow, S, component.[82] The input to the sensory neuron is given by

$$I_s = F - S$$

The fast component integrates over a sensory stimulus C with a characteristic rate α and decay rate β

$$\frac{dF}{dt} = \alpha C - \beta F.$$

The slow component moves towards the fast component with a delay

$$\frac{dS}{dt} = \gamma(F - S).$$

The intermediate neurons AIB, AIA, AIY were modelled according to the approach in.[82] All neurons are modelled as leaky integrators:

$$\tau_m \frac{dV_i}{dt} = -V_i + tanh(I),$$

where V_i is the voltage or activity of neuron i, τ_m is a time constant, $V_{0,i}$ is the resting potential and I is an input term. The input term is a sum over all inputs to a neuron $I = \sum_j w_{ij} V_j$. The parameter values were $\alpha = 4s^{-1}, \beta = 15s^{-1}, \gamma = 2s^{-1}, t_m = 0.5s$[82]

AIB activation is known to correspond to reorientation behaviour in the worm and AIY activation to cause the worm to move forwards along its current trajectory. To include this in the model the worms make stochastic decisions in each modelled time step to either continue going straight forward or to reorient to a new, random orientation. The probability of reorientation is governed by the response neuron R which is influenced by the activation of AIB and AIY. At each time step the worm can choose to continue moving forward on its current direction or to reorient itself by choosing a new random direction uniformly from 0-360 degrees. This decision is made by the reorientation neuron R, the output of which is

$$R = \tanh(w_8 V_{AIB} + w_9 V_{AIY}).$$

To make a reorientation decision a random number is drawn uniformly between -1 and 1. If this number is lower than R the worm will reorient, otherwise the worm will continue moving in its current direction.

Worm movement was simulated on a circular plate with radius 30 mm using the forward Euler method with a timestep $dt = 0.005s$. A worm starts at position (0,0) with an initial direction of motion, θ, drawn uniformly from 0–360 degrees. Worms move with a speed of $v = 0.11mms^{-1}$,[82] and at every timestep a reorientation decision is made. If the worm decides to reorient a new direction of motion is sampled from 0–360 degrees and the worm starts moving in this direction, otherwise the worm continues on its current direction of motion. The concentration of odour is given by a gaussian function with origin at (4.5, 0) and standard deviation of 4mm $C(x,y) = 100 * N(4.5, 0, 4)$.

To compare the simulated worms to the real worms a fitness function (F) was constructed using summary statistics of the distribution of sectors visited by the simulated and real worms. The score of a worm is the sum of all sectors that it visited. The range of a worm is the difference between the highest and lowest sector visited. The fitness function of a set of weights is based on the mean, standard deviation and skew of the score and the mean, standard deviation and skew of the range of the worms in a simulated experiment compared to the real data.

$$F_{score} = (mean(scores_{sim}) - mean(scores_{real})) + (std(scores_{sim}) - std(scores_{real})) + skew(scores_{sim}) - skew(scores_{real})$$

$$F_{range} = (mean(ranges_{sim}) - mean(ranges_{data})) + (std(ranges_{sim}) - std(ranges_{data})) + (skew(ranges_{sim}) - skew(ranges_{data}))$$

$$F = F_{score} + F_{range}$$

First data for 92 worms with no odour applied was used to find an effective sampling time for the worms. Simulated experiments of 92 worms were carried out for sampling time [0.06, 0.07, 0.08, 0.09, 0.10, 0.11, 0.12, 0.13, 0.14] seconds (Figure S5C). A sampling time of 0.10 was found to have the highest fitness and therefore was used as the sampling time for all subsequent simulations.

The method to fit the weights of the neural network to different behaviours is shown in Figure S5D. The target behaviour is defined by 212 behavioural assay data points of mock conditioned worms. The evolutionary algorithm starts from a population of randomly initialised weights, however w_8 was always set to 1 and w_9 to -1. During each round of evolution, the fitness of each set of weights in the population was calculated by carrying out a simulated experiment and calculating the fitness of the weights. The population was then ranked according to fitness. The top 40% of the population is left unchanged to go onto the next generation. The next 40% of the population is replaced by the top 40% after each weight has been perturbed by small random numbers. The final 20% of the population is replaced by new randomly sampled weights. The output of the evolutionary algorithm is the final population of weights. For all simulations the population size was 100 and it was evolved for 100 generations.

QUANTIFICATION AND STATISTICAL ANALYSIS

Calcium imaging analysis

A moving region of interest in both channels was identified and mean fluorescent ratios (GFP/RFP) were calculated with custom-made Matlab scripts by the de Bono lab.[83] All further analysis was performed using our own custom-made Matlab scripts. For RIA neurons, where photobleaching was evident, bleach-correction was applied independently to each channel by fitting an exponential decay curve to the raw fluorescence signal and dividing the signal by its fitted exponential.[84] Ratios were smoothened using a 5-frame rolling median. Baseline-adjusted ratios were calculated as (R-R0)/R0, where R0 is the average ratio during the baseline period (10s prior to odour presentation for AIY and RIA, and 10s prior to odour removal for RIM and AIB). Normalised ratios were calculated as (R-Rmin)/Rmax, where Rmin and Rmax are the average of the smallest and largest 5% of values in that trace,

respectively. For AIB and RIM, normalised ratios were calculated in order to classify neurons as being in either their ON or OFF state (classed as ON if (R-Rmin)/Rmax > 0.5, as per,[24,26] and then baseline-adjusted ratios were plotted to show differences in magnitude of response across conditions.

Imaging of EGL-4 subcelluar localisation

Animals were first subjected to one of the four conditioning protocols in the same way as for behavioural analysis. Immediately after conditioning, animals were split in two groups. One group was imaged for EGL-4 localization and the other group was tested for chemotaxis to benzaldehyde. Imaging of GFP-tagged EGL-4 was performed with a Zeiss Axio Imager 2 microscope, a Zeiss ECPLAN-NEOFLUAR 100x/1.3 oil immersion objective and TimeToLive 10_2016 Caenotec software. Animals were immobilised with 3μl of NaN_3 at a concentration of 25mM. AWC neurons were identified by expression of *odr-1::dsRed*, morphology and position. Z-stack images were taken for each animal and analysed using ImageJ blindly to the conditioning that the worms had been subject to. Average green fluorescence intensity at nuclear and cytoplasmic locations was calculated by drawing a polygon containing each region of interest (ROI) on the middle section of the z-stack for each AWC neuron and the ratio was calculated. Animals with ratios ≥ 1,4 were classified as having EGL-4 nuclear translocation.

Worm tracking

Videos of 10 minutes (during conditioning and exploration post-conditioning) or 20 minutes (chemotaxis post-conditioning) were taken at 15 frames per second using the Motif Video Recording System from Loopbio. Locomotion features were extracted and defined using Tierpsy Tracker as described in Javer et al. (2018).[73] Worms with missing skeletons for more than 50% of frames were excluded from the analysis. Because Tierpsy cannot resolve worms in contact, manual scoring using the QMplay2 video player was performed to analyse locomotion of males during sexual conditioning. For automated analysis, a sample of 10 videos per mock and aversively conditioning groups were manually checked for potential annotation mistakes made by Tierpsy. A cut off point of 80 frames (6.67 seconds) was decided as an upper limit for genuine reversal length (76% of reversals between 37.5 and 80 frames were manually scored as genuine reversals, whereas only 33% of reversals above 80 frames were genuine). A cut off point of 15 frames (1 second) was chosen as the lower limit for reversal length (83% of reversals between 15–25 frames were genuine based on Gray et al. 2005's description of R1 reversals – head bend followed by a change in direction of at least 40 degrees[41]). As Tierpsy fails to skeletonise worms in which head and tail are touching, omega turns could be reliably identified (89% of cases) as periods of missing data between 45 and 400 frames length preceded by negative speed.

Statistical analysis

For behavioural assays, because chemotaxis scores are discrete categorical data, χ^2 for trend analysis was used to compare the frequency distribution of values of different conditions. Bonferroni corrections were applied to account for multiple comparisons-derived false positives. For graphs of violin plots showing chemotaxis scores, each empty circle represents the score of an individual animal. White cross represents the mode. Black asterisks correspond to comparisons between conditions within genotype; green and red asterisks correspond to comparisons between genotypes for aversive and sexual conditioning, respectively. *** p< 0.001; ** p< 0.01; * p<0.05; n. s. no statistically significant difference p≥0.05. n, number of animals. At least 3 independent experiments were done for each group.

For CaMPARI photo conversion, a non-parametric two tailed Mann Whitney-U test was performed. For graph showing CAMPARI photoconversion (Figure 3E), each circle represents a neuron. ***p<0.001; ** p<0.01, * p<0.05. Error bars represent SEM. n, number of neurons.

For baseline-adjusted GCaMP6f/RFP fluorescence ratios analysis between conditions, non-parametric one-way ANOVA (Kruskal Wallis test) with Dunn's multiple comparisons was performed because the data did not follow a normal distribution. For RIA axonal domains comparisons were made during the second odour exposure (70-75 seconds). * p<0,05; n.s. no statistically significant difference p≥0.05. 32 neurons were analysed for mock, 23 for aversive, and 24 for sexual conditioning for RIA nrd. 26 neurons were analysed for mock, 24 for aversive, and 31 for sexual conditioning for RIA nrv. 28 neurons were analysed for mock, 23 for aversive, and 26 for sexual conditioning for RIA loop. For AIB and RIM, only neurons with low activity (normalised fluorescence R- Rmin/Rmax <0.5) before odour removal were selected. For AIB, 75 neurons were analysed for mock, 42 for aversive, and 48 for sexual conditioning. For RIM axon, 36 neurons were analysed for mock, 29 for aversive, and 40 for sexual conditioning. To compare maximum activity in AIB and RIM neurons during odour removal (60 sec) (Figures 4D and 4E middle), non-parametric ANOVA test was used to compare conditions. Each dot represents one neuron. Black lines represent the average. n. s. no statistically significant difference p≥0.05. To compare the effect of conditioning on the proportion of active neurons (Figures 4D and 4E right), we used a binary logistic regression (generalised linear model with a logit link and the binomial family), and compared the full model (activity ~ condition + time) with the partial model (activity ~time), using an ANOVA, in order to evaluate the effect of condition. **** p< 0.0001; * p< 0.05. For all GCaMP imaging at least three independent experiments were done for each condition.

For activity in the axon of AIY (Figures 6A and 6B), responses were analysed as normalized GCaMP6f/RFP fluorescence ratios $(R\text{-}R_{min})/R_{max}$ and plotted as heat maps for each neuron (Figure 6A) or as average traces for type 1 and type 2 responses (Figure 6B). 29 neurons were analysed for mock, 24 for aversive, and 75 for sexual conditioning for AIY wild type. 35 neurons were analysed for mock, 36 for aversive, and 50 for sexual conditioning for AIY *pdf-1(tm1996)*. χ^2 test was used to compare the proportion of type 2 responses in AIY between conditions and genotypes. ** p< 0.01. At least 3 independent experiments were performed for each group.

For comparison of reversal and omega turn frequency, and proportion of time moving forward during conditioning (Figure 5B and Figure S2A), a non-parametric ANOVA test (Kruskal-Wallis) with multiple comparisons was performed. For comparison of the distribution of reversal length between conditions, a χ^2 for trend analysis was used, using the deciles of mock reversals as bin edges to determine categories. In those graphs, each dot represents an event and black lines represent the mean. * $p<0.05$; n. s. no statistically significant difference $p \geq 0.05$. n = number of animals.

To compare EGL-4 nuclear translocation between different conditioning groups (Figure 5C) a χ^2 test with Bonferroni corrections was used to account for multiple comparisons derived false positives. Black asterisks show statistically significant difference between conditioning types. *** $p< 0.001$; n. s. no statistically significant difference $p \geq 0.05$. n= number of neurons